Effect of regional-scale transport on oxidants in the vicinity of Philadelphia during the 1999 NE-OPS field campaign

Jerome D. Fast, Rahul A. Zaveri, Xindi Bian, Elaine G. Chapman, and Richard C. Easter

Pacific Northwest National Laboratory, Richland, Washington, USA

Received 25 June 2001; revised 28 January 2002; accepted 28 January 2002; published 28 August 2002.

[1] A new meteorological-chemical model is used to determine the relative contribution of regional-scale transport and local photochemical production on air quality over Philadelphia. The model performance is evaluated using surface and airborne meteorological and chemical measurements made during a 30-day period in July and August of 1999 as part of the Northeast Oxidant and Particulate Study (NE-OPS). Good agreement between the simulations and observations was obtained. The bias in the vicinity of Philadelphia over the simulation period was −5.8 ppb for the peak ozone mixing ratio during the day and 2.0 ppb for the minimum ozone mixing ratio at night. Layers of ozone above the convective boundary layer were measured by both research aircraft and ozonesondes during the morning between 0900 and 1100 LT. The model demonstrates that upwind vertical mixing processes the previous afternoon, subsequent horizontal transport aloft, and depletion of ozone by NO titration within the stable boundary layer at night lead to the development of these layers. Ozone aloft was then entrained into the growing convective boundary, contributing to surface ozone concentrations. Through a series of sensitivity studies, we find that most of the ozone is the result of emissions in the vicinity of Philadelphia and Chesapeake Bay area, but up to 30–40% of the ozone during high ozone episodes was due to transport from upwind sources. Local emissions and meteorological conditions were largely responsible for one high ozone episode because of light winds. *INDEX TERMS:* 0345 Atmospheric Composition and Structure: Pollution—urban and regional (0305); 3307 Meteorology and Atmospheric Dynamics: Boundary layer processes; 3337 Meteorology and Atmospheric Dynamics: Numerical modeling and data assimilation; *KEYWORDS:* boundary layer, regional-scale transport, mesoscale meteorological model, chemical transport model

Fast, Jerome D.; Zaveri, Rahul A.; Bian, Xindi; *et al.* 2002. Effect of regional-scale transport on oxidants in the vicinity of Philadelphia during the 1999 NE-OPS field campaign. Journal of Geophysical Research. 107(D16): ACH 13-1—ACH 13-22.

1. Introduction

[2] A stumbling block in understanding the processes contributing to high ozone events is the lack of routine trace gas observations aloft that provide evidence relevant to regional-scale transport. This is of special concern in the northeastern United States where it is thought that ozone formed from upwind sources contributes to local high ozone episodes [*Hidy*, 2000; *Solomon et al.*, 2000]. Local and regional transport of pollutants from one city to the next can occur frequently because of the proximity of the metropolitan areas along the coast. In addition, meteorological conditions in the summer are often favorable for transport from more distant sources located in the midwest and south. The role of transport on downwind ozone concentrations is also complicated by the fact that the chemistry connecting primary precursor pollutants such as NO_x ($NO + NO_2$) and volatile organic carbon compounds to secondary pollutants such as ozone is extremely complex [e.g., *Finlayson-Pitts and Pitts*, 2000; *Sillman*, 1999].

Copyright 2002 by the American Geophysical Union.
0148-0227/02/2001JD000980$09.00

[3] Most studies on the relationship of ozone and transport over the eastern United States have been performed using indirect evidence from meteorological analyses. Several techniques have been employed, such as trajectory clustering [e.g., *Brankov et al.*, 1998] and climatological analyses that determine the primary transport patterns associated with high ozone episodes [e.g., *Schichtel and Husar*, 2001; *Vukovich*, 1995]. Three-dimensional prognostic models have been used in conjunction with meteorological data to examine mesoscale transport processes, such as the Appalachian lee trough [*Seaman and Michelson*, 2000], that can affect ozone distributions in the northeastern United States. Other studies have estimated the export of ozone from specific urban areas that will subsequently affect downwind rural and urban areas [e.g., *Duncan and Chameides*, 1998; *Hidy*, 2000].

[4] Several field campaigns have been conducted along the east-coast urban corridor, such as the North American Research Strategy for Tropospheric Ozone (NARSTO) Northeast field campaigns in the summers of 1995 and 1996 [*Solomon et al.*, 2000], to measure trace gas species aloft and provide episodic observations of air pollutant transport. Research aircraft have measured ozone and other pollutants within urban plumes over the northeastern United

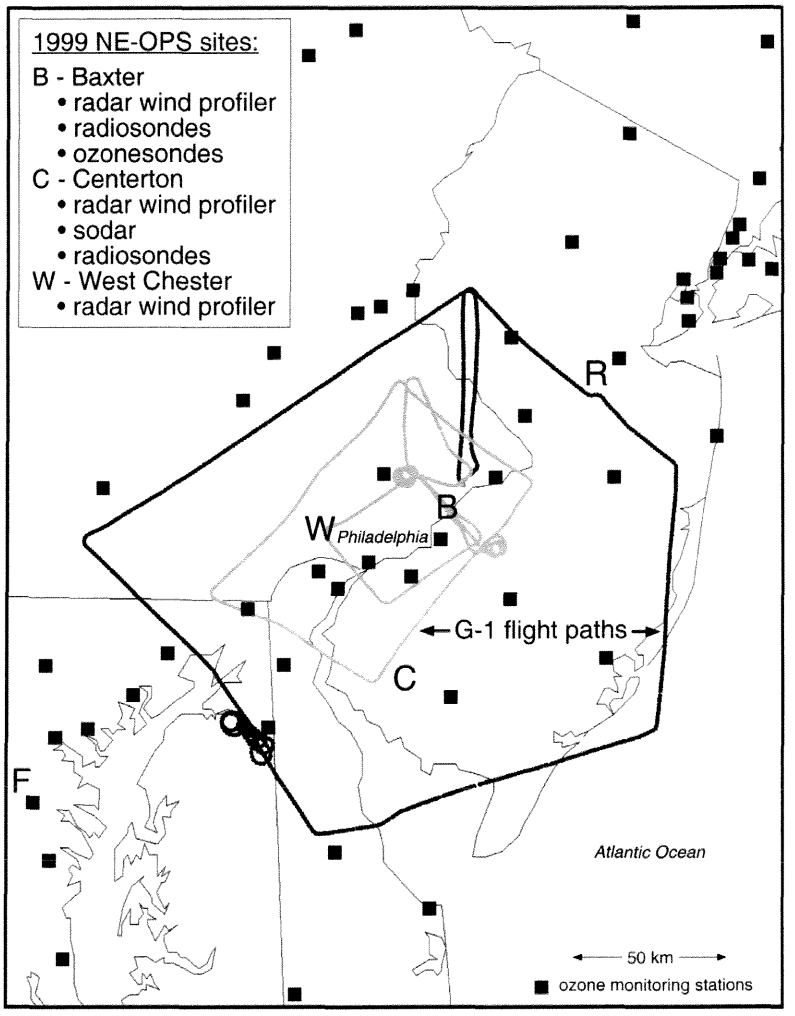

Figure 1. Locations of the Baxter (B), Centerton (C), and West Chester (W) instrumentation sites during NE-OPS. Operational radar wind profiler measurements were available from the Fort Meade (F) and Rutgers University (R) sites. Two flight paths of the G-1 aircraft are shown to illustrate the horizontal extent of chemical measurements aloft (black line denotes "regional" and shaded line denotes "regional-to-local" as listed in Table 1).

States [*Berkowitz et al.*, 1998; *Kleinman et al.*, 2000; *Van Valin et al.*, 1994; *Zhang and Rao*, 1999] and in many other locations in North America [e.g., *Banta et al.*, 1998; *McKendry et al.*, 1997]. During the morning, ozone concentrations aloft are sometimes significantly higher than observed by surface ozone monitoring stations. These ozone layers contribute to surface concentrations when they are entrained into the growing convective boundary layer [e.g., *Fast et al.*, 2000; *McElroy and Smith*, 1993; *Neu et al.*, 1994].

[5] More recently, the 1999 Northeast Oxidant and Particulate Study (NE-OPS) was conducted during July and August in the vicinity of Philadelphia. The purpose of the field campaign was to investigate the conditions leading to high ozone and particulate concentrations in the urban environment, determine the contributions from local and distant sources, and examine the role of meteorological properties on the buildup and distribution of pollutants over urban and regional scales. Some of the measurements have been described by *Clark et al.* [2001], *Doddridge* [2000], and *Philbrick et al.* [2000]. The surface and upper-air observations provide valuable information that can be used to evaluate the performance of meteorological and chemical models in simulating transport of pollutants. For example, wind profiler data have been used to investigate the effect of boundary layer parameterizations on the evolution of low-level jets [*Zhang et al.*, 2001] and ozone [*Ku et al.*, 2001] observed on four consecutive days of July 1999.

[6] Few modeling studies, however, have quantified the relative contributions of upwind sources on ozone concentrations in the northeast [*Hidy*, 2000]. In this paper, we discuss instrumentation deployed during the 1999 NE-OPS field campaign in section 2.1 not reported previously. Some of the observations are shown in section 2.2 to illustrate periods where ozone was transported into the Philadelphia area and describe the principal boundary layer features relevant to entrainment of ozone into the convective boundary layer. We also describe a new meteorological and chemical model in section 3 that is employed to investigate the relative role of local and regional-scale processes that

Table 1. List of Flight Times and Flight Paths of G-1 Aircraft During 1999 NE-OPS Field Campaign[a]

Flight	Date	Time, LT	Type of Flight Path
1	23 July	1447–1602	local
2	25 July	0933–1059	local
3	26 July	1340–1623	regional
4	27 July	0933–1207	local
5	27 July	1340–1558	local-to-regional
6	29 July	1338–1624	regional
7	30 July	1334–1608	local-to-regional
8	31 July	0940–1159	local
9	31 July	1339–1602	local-to-regional
10	1 August	0934–1152	local
11	1 August	1340–1528	local-to-regional
12	3 August	1331–1559	regional
13	4 August	1347–1605	local-to-regional
14	5 August	0937–1203	local
15	5 August	1351–1527	local
16	7 August	0933–1157	local
17	7 August	1339–1541	local-to-regional
18	10 August	0935–1135	local
19	10 August	1341–1548	local-to-regional
20	11 August	0952–1140	local

[a] Typical "regional" and "local-to-regional" flight paths are shown in Figure 1. A "local" flight path usually consists of one transect around Philadelphia and one or more horizontal transects northeast of Philadelphia.

affect multiple high ozone episodes over a 30-day period. The results of the model are presented in section 4, and the impacts of model assumptions on the simulation results are discussed in section 5. In a subsequent paper we will extend our analysis to resolve small-scale processes and emissions using a 4-km grid that encompasses the east-coast urban corridor between Washington, D. C., and New York City.

2. Field Campaign Measurements

2.1. Instrumentation

[7] Researchers from the U.S. Department of Energy's (DOE) Argonne National Laboratory (ANL), Brookhaven National Laboratory (BNL), and Pacific Northwest National Laboratory (PNNL) participated in the NE-OPS field campaign between 23 July and 11 August 1999. During the 1999 experiment, the normally available surface meteorological measurements were supplemented with additional data collected from an array of radar wind profilers, a sodar, and radiosondes. Additional chemical measurements were obtained from routine surface monitoring stations and from the DOE's Gulfstream-1 (G-1) aircraft.

[8] Twenty flights were made by the G-1 aircraft on 14 days during the field campaign to obtain ozone, CO, NO, NO_y (defined as $NO_x + NO_z$ where NO_z represents all NO_x oxidation products, for example, HNO_3, HONO, NO_3 radical, N_2O_5, PAN, etc.), and particulate data aloft. The primary objective of the G-1 flights was to characterize the chemistry near the source of local emissions and to sample the same parcels of air as they were transported downwind. A morning (between 0900 and 1200 LT) and an afternoon (between 1300 and 1600 LT) flight were made on six of these days. Typical flight paths are shown in Figure 1, and a list of flight times is given in Table 1. Three different flight paths were completed. An outer "regional" flight path (the black line in Figure 1) was made on 3 days. The flights on the rest of the days consisted of two "local-to-regional" transects around Philadelphia (the gray line in Figure 1) or "local" variations that consisted of one transect around Philadelphia and transects to the northeast of the city. The University of Maryland also operated a small research aircraft on 30 and 31 July and 1 August [*Doddridge*, 2000] during the G-1 operational period.

[9] The locations of the measurement sites used for boundary layer profiling are also shown in Figure 1. Three 915 MHz radar wind profilers were located at sites denoted by B, C, and W. Site B (Baxter) was located in the urban area along the Delaware River approximately 18 km northeast of downtown Philadelphia. Site C (Centerton) was located in a rural area about 50 km south of site B. Site W (West Chester) was located in a suburban area on the campus of West Chester University, about 35 km west of site B. Sites C and W were chosen to bracket the expected path of the urban plumes transported over Philadelphia by southwesterly flow associated with a Bermuda high. Each profiler was configured to operate in two modes, a high resolution one with 60-m range gates and a lower resolution mode with 100-m range gates. Good data recovery was obtained to altitudes of over 3 km at each of the profilers. Each profiler was also equipped with a radio acoustic sounding system to obtain virtual temperature profiles to altitudes of about 1 km. Hourly wind speeds and directions were obtained at sites C and W between 23 July and 11 August while data were obtained throughout July and August at site B. At site C, a sodar also provided wind measurements at a resolution of 5 m to heights of approximately 130 m. Two operational radar wind profilers at sites F (Fort Meade) and R (Rutgers University) provided additional wind profiles along the mid-Atlantic coast.

[10] At two of the radar profiler sites (B and C), radiosondes were released five times per day on days during which the G-1 aircraft was making measurements. The release times were 0800, 1000, 1200, 1400, and 1700 LT (1200, 1400, 1600, 1800, and 2100 UTC). The sondes measured wet and dry bulb temperatures and pressure. A single sonde launch was generally performed on other days at 1700 LT to obtain a measurement of the depth of the late afternoon mixed layer. The height of the mixed layer often reached 3 km. These mixed layers were deeper than expected, probably due to the dry conditions during the summer of 1999. Some spatial variations in the mixing layer depth were also observed when comparing the potential temperature profiles from sites B and C. There were a few days in which the mixed layer depth was higher over the urban area; however, there were no systematic differences between sites B and C. At site B, Millersville University used a tethersonde to obtain more frequent profiles of temperature, humidity, wind, and ozone within 300 m of the ground on several days [*Clark et al.*, 2001], and Pennsylvania State University operated a Raman lidar to obtain humidity profiles up to 6 km [*Philbrick et al.*, 2000].

[11] PNNL launched one EN-SCI Corporation electrochemical concentration cell (ECC) ozonesonde [*Komhyr*, 1969; *Komhyr et al.*, 1995] per day between 2 and 11 August from site B. Most of the ozonesondes were released in the morning between 1000 and 1100 LT as indicated by the list of launch times given in Table 2. While the objective was to supplement aircraft measurements by obtaining vertical ozone profiles within and above the growing con-

Table 2. List of Ozonesonde Launch Times From Baxter Site

Sonde	Date	Time, LT
1	2 August	1800
2	3 August	1400
3	4 August	1220
4	5 August	1040
5	6 August	1020
6	7 August	1000
7	8 August	1015
8	9 August	1000
9	10 August	1000
10	11 August	1000

vective boundary layer, the ozonesonde measurements also extended up to an altitude of about 20 km.

2.2. Observations

[12] Hourly meteorological and ozone measurements at the surface were obtained from operational monitoring networks. The locations of the U.S. Environmental Protection Agency's Aerometric Information Retrieval System (AIRS) ozone monitoring stations in the vicinity of Philadelphia are shown in Figure 1. One-minute ozone measurements were made at site B, and measurements of ozone, nitrogen oxides, PAN, and particulate matter were made at site C [*Marley et al.*, 2001].

[13] Figure 2a depicts hourly averaged ozone measured at eight stations within 35 km of site B. Ozone mixing ratios in the area met or exceeded the 1-hour National Ambient Air Quality Standard (NAAQS) of 120 ppb on 5 days between 15 July and 14 August. The high ozone episodes were usually associated with relatively higher temperatures and humidities (Figure 2b) and mostly clear skies (Figure 2c). Drought conditions were observed in the mid-Atlantic states during the summer of 1999 with temperatures 2 to 3 K above normal. Precipitation occurred in Philadelphia only on 3 days (19 July and 8 and 14 August) during this 30-day period.

[14] While the observations in Figures 2b and 2c suggest that local meteorological conditions were correlated with the development of the high ozone episodes, regional-scale transport of ozone and ozone precursors may have also played a role. Philadelphia is located in a region with a multitude of mobile and point sources of pollutants. Winds in the Philadelphia area are generally from the south and west during the summer months. Pollutants can be transported from other urban areas upwind of Philadelphia along the urban east-coast corridor (e.g., Baltimore and Washington, D. C.) or from sources in the midwest (e.g., Ohio River valley).

[15] There were two periods, 5 and 11 August, during which the upper-air meteorological and air chemistry measurements indicated that regional-scale transport of ozone into Philadelphia likely occurred. While there were other days with higher peak ozone mixing ratios, there were either insufficient air chemistry observations aloft or the measurements made during the morning did not contain distinct layers of ozone just above the growing convective boundary layer (CBL).

[16] Sample meteorological and ozone measurements for the first period on 5 August are shown in Figure 3. The potential temperature profiles (Figure 3a) reveal that the shallow CBL observed at 0800 LT grew gradually over the next 3 hours to a height of 0.75 km. Between 1100 and 1200 LT, the CBL grew dramatically to 1.75 km, finally reaching a maximum height of 2.25 km in the late afternoon. The ozonesonde released at 1040 LT measured relatively uniform mixing ratios between 40 and 45 ppb within the CBL and a layer of ozone aloft just above the CBL with peak values around 80 ppb. Also shown in Figure 3b are the measurements from the G-1 aircraft between 0937 and 1203 LT. The complicated ozone distribution (Figure 3b) is the result of the aircraft flying within and above the growing CBL as well the spatial

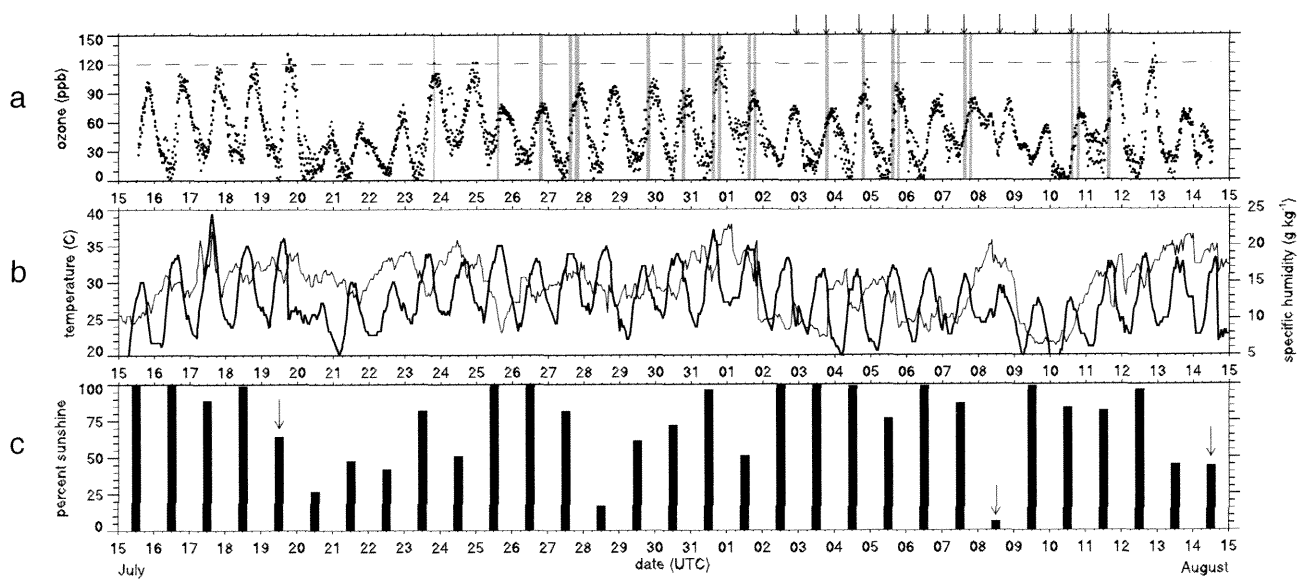

Figure 2. Time series of (a) ozone mixing ratio at monitoring stations within 25 km of site B, (b) temperature (thick line) and specific humidity (thin line), and (c) percent sunshine during the NE-OPS field campaign. Shaded lines and arrows in Figure 2a indicate G-1 aircraft flight periods and ozonesonde launch times, respectively. Arrows in Figure 2c indicate days with precipitation.

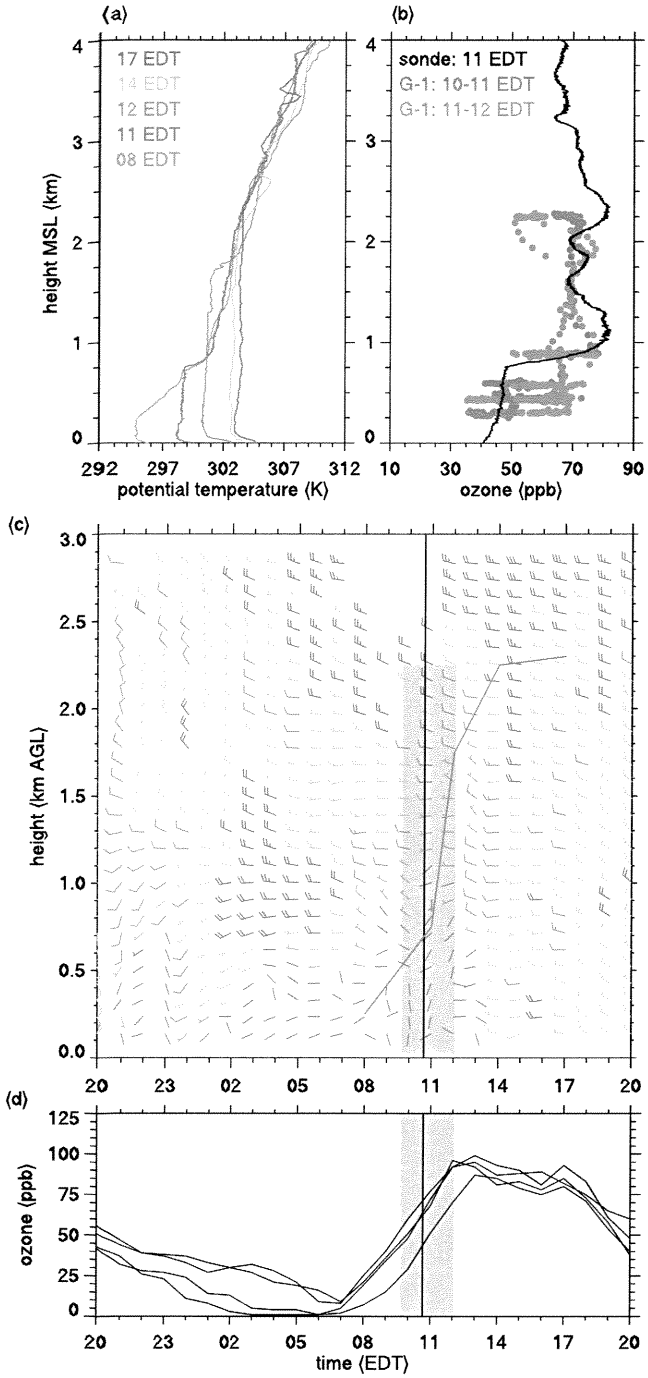

Figure 3. Observed (a) potential temperature, (b) ozone, and (c) wind profiles at site B and (d) hourly averaged surface ozone at monitoring stations within 25 km of site B on 5 August. Shading and vertical line in Figures 3c and 3d indicate G-1 aircraft flight period and ozonesonde launch time, respectively. Blue line in Figure 3c is the CBL height as determined from the profiles in Figure 3a. A full wind barb is 5 m s^{-1}.

inhomogeneity of ozone within 40 km of site B. Nevertheless, the vertical gradient of the G-1 ozone early in the flight (1000–1100 LT) is similar to the ozonesonde profile. One hour later (1100–1200 LT) the G-1 profile became more uniform as ozone was entrained into the growing CBL. The radar wind profiler (Figure 3c) indicates that a low-level jet with wind speeds up to 12.5 m s^{-1} at 1 km above ground level (AGL) was present during the early morning hours. The high wind speeds imply that the ozone layer aloft was transported a substantial distance and that it was not a residual layer of ozone produced by local emissions the previous afternoon.

[17] The second period of regional-scale transport is shown in Figure 4 for 11 August. On this day, the CBL only grew to about 1 km AGL by 1400 LT (Figure 4a). As in the previous case, uniform ozone mixing ratios around 55 ppb were observed within the CBL at 1000 LT, with a

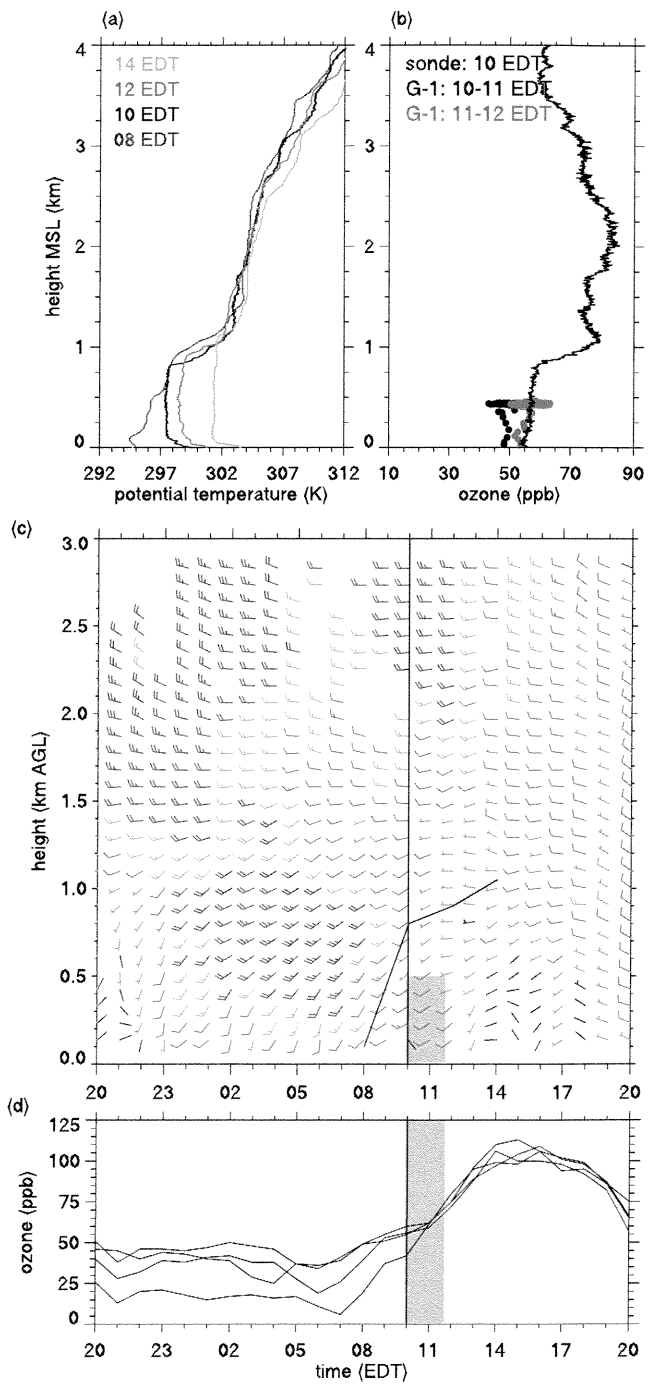

Figure 4. Same as Figure 3, except for 11 August.

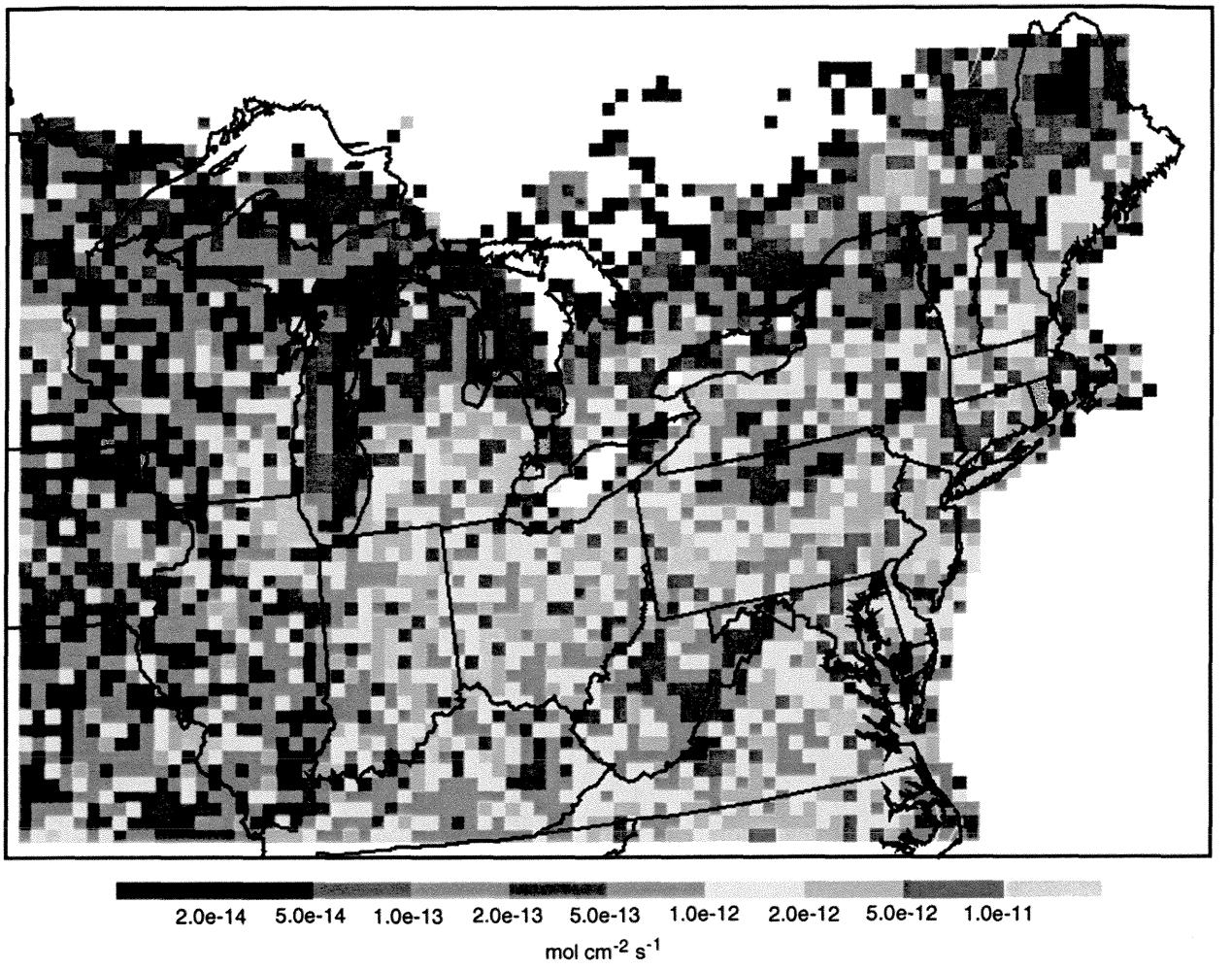

Figure 5. The second grid (x = 24 km) employed by the meteorological and chemical model with the CO emission rates at 1200 UTC on 15 July.

relatively deep layer of ozone between 70 and 75 ppb (Figure 4b) above the CBL. The G-1 flew only one horizontal transect around Philadelphia at 500 m AGL, but the measurements were consistent with the ozonesonde values. A low-level jet was also observed during the early morning (Figure 4c), but in contrast to the 5 August period, the winds were southwesterly with higher wind speeds observed closer to the surface.

[18] At the time of the aircraft and ozonesonde launch, surface ozone mixing ratios were increasing as shown in Figures 3d and 4d. Considering the higher ozone concentrations aloft it is likely that entrainment processes contributed to the surface concentrations in addition to chemical production; however, the observations are insufficient by themselves to quantify the effect of vertical mixing. Observational evidence of regional-scale transport on near-surface ozone concentrations on other days was not as obvious as on 5 and 11 August; however, that does not mean that regional-scale transport was not significant for other high ozone episodes during the NE-OPS field campaign. The role of horizontal transport and entrainment processes on surface ozone mixing ratios will be investigated in the following sections by employing a coupled meteorological and chemical model for 5 and 11 August and other periods where regional-scale transport was not clearly evident from the observations.

3. Model Description

[19] A model is employed to assist in the interpretation of the observations and to provide additional insights into the processes important to the transport and mixing of ozone in the region. In this section we briefly describe a model, the PNNL Eulerian Gas and Aerosol Scalable Unified System (PEGASUS), that consists of a mesoscale meteorological model and a chemical transport model. We then present some of the results and discuss their implications.

3.1. Mesoscale Meteorological Model

[20] Version 4.3 of the RAMS mesoscale model [*Pielke et al.*, 1992] was used to simulate the meteorological conditions between 1200 UTC 15 July and 1200 UTC 14 August. RAMS employs a two-way interactive nested grid structure, and in this study the model domain consisted of two grids. The first grid encompassed most of eastern North America with a grid spacing of 48 km. The second grid, shown in Figure 5, encompassed the north-

central and northeastern United States and southern Canada with a 24-km grid spacing. A terrain-following coordinate was used with a vertical grid spacing of 25 m adjacent to the surface that gradually increased to 600 m near the model top at 20 km. Due to the staggered vertical coordinate, the first grid point was 12.5 m AGL.

[21] The turbulence parameterization consists of a simplified second-order closure method that employs a level-2 diagnostic scheme and a level-2.5 scheme with a prognostic turbulence kinetic energy equation [*Mellor and Yamada*, 1982; *Helfand and Labraga*, 1988]. Although the cumulus and cloud microphysics parameterizations were not activated to produce precipitation, condensation of vapor to cloud water was simulated. The *Chen and Cotton* [1983] shortwave and longwave parameterizations that include cloud effects were used to determine the heating or cooling caused by radiative flux divergences. Turbulent sensible heat, latent heat, and momentum fluxes in the surface layer were calculated from similarity equations [*Louis*, 1979]. Prognostic soil-vegetation relationships were used to calculate the diurnal variations of temperature and moisture at the ground-atmosphere interface where vegetation type was based on a U.S. Geological Survey 1-km data set for North America. Soil moisture was initialized using values obtained from the National Center for Environmental Prediction's AVN model.

[22] Application of a four-dimensional data assimilation (4DDA) technique was necessary to limit the forecast errors in the meteorological fields over the long simulation period. In this study, 4DDA nudged the u- and v-components of the wind, the potential temperature, and the humidity in the boundary layer and free troposphere into closer agreement with the 6-hour analyses from the AVN model. A relaxation coefficient of 4.6×10^{-5} s^{-1} was used. The special meteorological observations made during the field campaign (Figure 1) were not incorporated by the 4DDA procedure so that they could be used as a independent data set to evaluate the model.

3.2. Chemical Transport Model

[23] The Eulerian chemical transport model used in this study is an updated version of the one described by *Berkowitz et al.* [2000] and *Fast et al.* [2000] that includes transport, vertical diffusion, chemical production/destruction, dry deposition, and emission terms. The gas-phase chemistry in PEGASUS is modeled with the newly developed photochemical mechanism CBM-Z [*Zaveri and Peters*, 1999] that contains 53 species and 133 reactions. CBM-Z employs the lumped-structure approach for condensing organic species and reactions, and is based on the widely used Carbon Bond Mechanism (CBM-IV) developed by *Gery et al.* [1989] for use in urban air-shed models. CBM-Z extends the original framework to function properly at larger spatial scales and longer time periods. Our motivation for using CBM-Z, relative to other carbon bond (or similar lumped) mechanisms is to benefit from its inclusion of reactive long-lived species and their intermediates, which may become important under conditions of transport at larger spatial scales and longer timescales. For example, peroxy radical interactions may become important under low NO_x conditions. The major differences with CBM-IV include revised inorganic chemistry, explicit treatment of lesser reactive paraffins such as methane and ethane, revised parameterizations of the reactive paraffin, olefin, and aromatic reactions, inclusion of alkyl and acyl peroxy radical interactions and their reactions with the NO_3 radical, inclusion of longer-lived organic nitrates and hydroperoxides, and refined isoprene chemistry. The version of CBM-Z used in this study contains an additional lumped species ANOL, which represents ethanol and higher alcohols, and its reaction with OH to take advantage of ethanol emission rates that were available. The numerical aspects of the chemical transport model are given in Appendix A.

[24] The domain for the chemical model coincided with the inner grid of RAMS shown in Figure 5. While the meteorological grid extended up to 20 km AGL, chemistry was simulated up to 6 km AGL. Hourly meteorological fields (u, v, and w components of the wind, temperature, humidity, eddy diffusivity, fractional area cloud coverage, and surface properties) were obtained from the mesoscale model. The initial and lateral boundary conditions for ozone were based on climatological profiles and the observed ozonesonde profiles during NE-OPS. The ozonesonde values above 3 km AGL were 10 to 30 ppb larger than climatological values so an average of the two was used at these elevations. Since the ozonesonde measurements near the ground are representative only of the local environment, the climatological values were used as boundary conditions near the surface. Ozone varied from 25 ppb at the ground to 50 ppb at 5 km AGL. The initial conditions for the other trace gas species were assigned to low background values, and the concentrations of all species were held constant at the boundaries during the simulation period. A zero-gradient condition was employed so that the lateral boundary conditions for ozone and other species affect the interior fields when the flow is into the domain.

[25] Hourly emission rates of 14 species were obtained from the Sparse Matrix Operator Kernel Emissions (SMOKE) model [*Houyoux et al.*, 2000]. SMOKE takes "raw" emissions data such as source locations, stack parameters, speciation profiles, and meteorological conditions for point, area, mobile and biogenic source categories to produce spatially and temporally distributed emissions over the continental United States and southern Canada. For this study, the emissions were based on the meteorology from the RAMS simulation that varied hourly over the 30-day period. The SMOKE emissions were generated off-line on a 4-km grid over the eastern United States and Canada, using RAMS meteorological values from the inner nested grid interpolated to the 4-km grid. The emissions were then aggregated to the 24-km grid spacing used by the PEGASUS simulation. CO emissions at 1200 UTC 15 July, a Thursday, are shown in Figure 5 to illustrate the spatial distribution over the modeling domain. Somewhat lower anthropogenic emission rates were obtained on weekend days relative to weekdays. The magnitude of the isoprene emissions in the vicinity of Philadelphia reflects the daily variation in temperature shown in Figure 2b. Emissions were vertically resolved by SMOKE for the lowest eight layers of PEGASUS. Emissions above the first layer are primarily from point sources, such as those from power plant stacks.

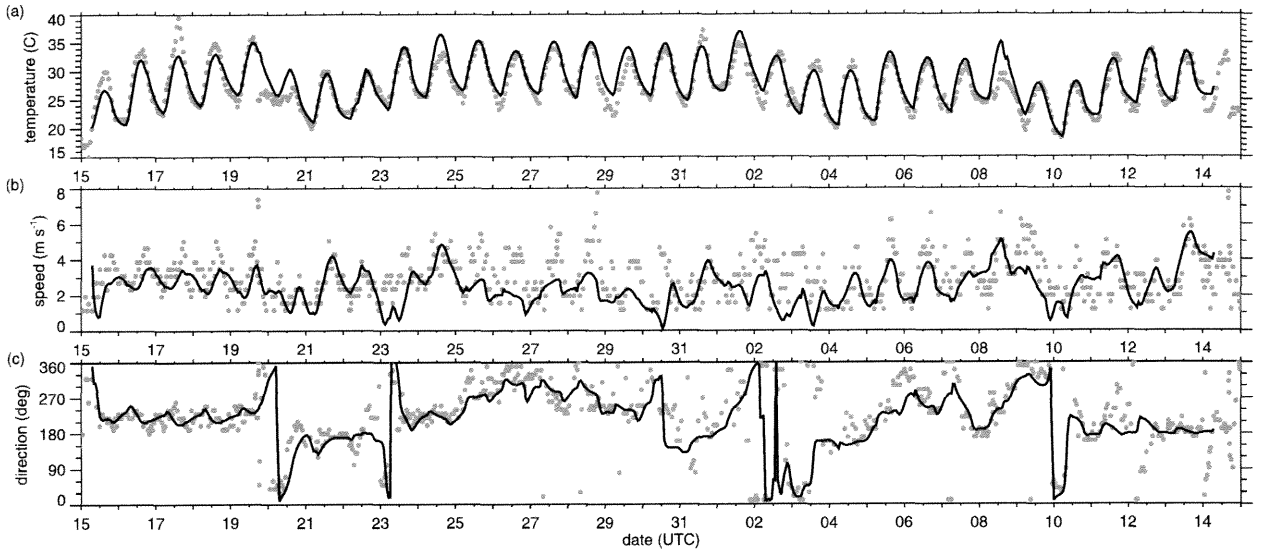

Figure 6. Time series of the observed (shaded dots) and simulated (lines) surface (a) temperature, (b) wind speed, and (c) wind direction at Philadelphia.

[26] Large-scale cloud fields were allowed to form in RAMS based on a diagnostic scheme that is a function of supersaturation. The associated mixing of trace gases with these large-scale cloud fields was reflected in modifications to the vertical velocity and turbulent kinetic energy (and thus eddy diffusivity) fields. Thus, large-scale cloud mixing was included, but sub-grid cloud mixing (e.g., fair weather cumulus) was not. Photolysis rates were modified by clouds, similar to work by *Chang et al.* [1987], using the fractional area cloud coverage.

4. Results

[27] We first present a comparison of the observed and simulated meteorological and chemical values during the 1999 NE-OPS field campaign, using performance measures that are common in the literature. The model run described in the previous section is referred to as the control simulation. The results of a series of sensitivity simulations are then presented to quantify the role of regional-scale transport of pollutants relative to local sources in the vicinity of Philadelphia during the 30-day period in addition to the 5 and 11 August cases described in section 2.2.

4.1. Boundary Layer Properties

[28] The simulated meteorological fields were compared with surface observations over the model domain, and profiles of wind, temperature, and humidity were made in the vicinity of Philadelphia. An example of the observed and predicted surface quantities for Philadelphia is shown in Figure 6. The model reproduced the diurnal and multiday variation in the surface temperature well. There are only a few days where the temperature was overpredicted (20 and 24 July and 8 August) or underpredicted (17 and 31 July). The predicted wind speeds and directions are similar to the observations, except that the simulated peak wind speeds during the afternoon are too low on most days.

[29] It is more important, however, to obtain reasonably accurate winds above the surface when evaluating regional-scale transport of pollutants. Since the model employs 4DDA, the meteorological fields followed the synoptic patterns during the 30-day period. The winds aloft were evaluated by comparing the simulated results with the radar wind profiler winds that were not employed by 4DDA. Data from the Baxter profiler was available 83% of the hours during the simulation period. The bias in the wind speed and direction at the Baxter site is shown in Figure 7. On average, the model winds were slightly higher than observed 300 m AGL and about 1 m s^{-1} too low above 0.75 km AGL. The simulated directions were usually more westerly than observed by 10° to 15°. The wind direction errors were largest at the surface and decreased with height. The overall errors for each of the five radar wind profiler

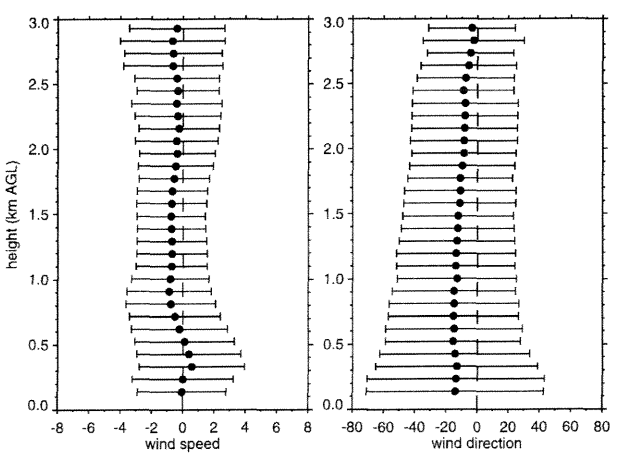

Figure 7. Mean (dots) and standard deviation (lines) of the bias *simulated − observed* in the wind speed and direction for the radar wind profiler range gates at site B based on 598 hours of data (out of a possible 721).

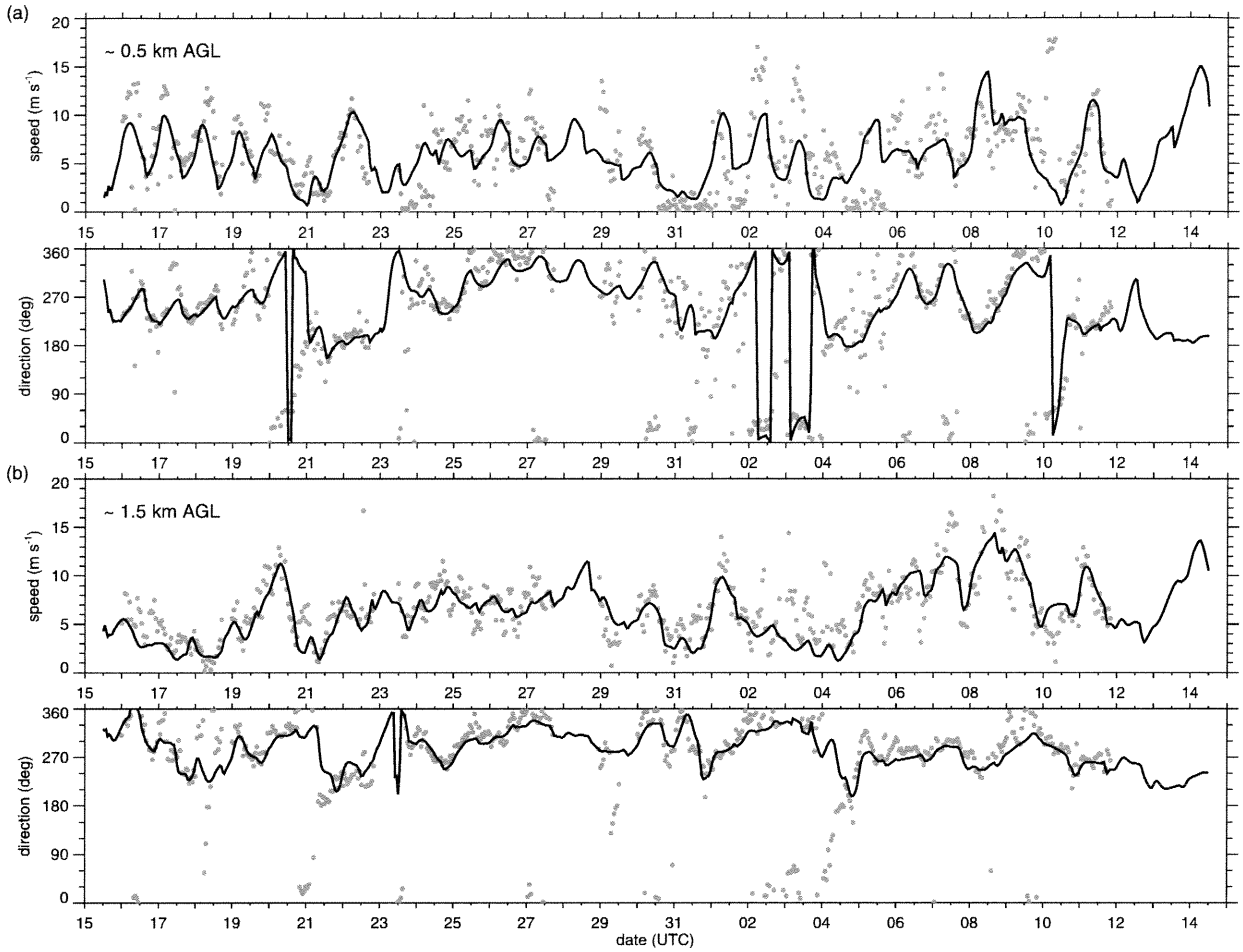

Figure 8. Time series of the observed (shaded dots) and simulated (lines) wind speed and direction at (a) 0.5 km and (b) 1.5 km AGL at site B.

sites were small, and the statistics shown in Figure 7 are similar to those reported by *Zhang et al.* [2001] for their MM5 simulation of the 15–19 July 1999 episode that employed a 12-km horizontal grid spacing.

[30] A more intuitive comparison is given in Figure 8 by the time series of wind speed and direction at the radar wind profiler range gates closest to 0.5 and 1.5 km AGL. At 0.5 km AGL, the model predicted the observed trends in speed and direction throughout the 30-day period. On several days, however, the simulated peak wind speeds were too low, similar to the behavior at the ground (Figure 6b). For example, on the evenings of 16–18 July, a low-level jet formed between 0.4 and 0.8 km AGL. The height of the low-level jet in the model was about the same as observed by the radar wind profiler, but the peak wind speeds were 3–4 m s^{-1} lower than the observed speeds of 13 m s^{-1}. At 1.5 km AGL, the wind speeds and directions were almost always in close agreement with the observations since the winds at this level are influenced more by synoptic forcing. The winds at 1.5 km AGL were generally from the west, while the winds closer to the surface at 0.5 km AGL were more frequently from the southwest. The vertical wind direction shear suggests that regional-scale pollutant transport from multiple upwind sources could potentially impact the Philadelphia area at the same time. This will be discussed later in section 4.3. The upper level winds at sites B, C, and W were usually very similar to those shown in Figure 8b throughout the period. Significant differences in the winds among the three sites occurred only when the synoptic forcing was weak.

[31] The simulated thermodynamic quantities, such as potential temperature, specific humidity, and mixed layer depth, were also evaluated with the radiosonde observations at site B. Instead of depicting individual profiles, Figures 9a and 9b compare the observed average potential temperature and specific humidity since these are usually relatively uniform within the CBL. In this way, values from 65 soundings made between 23 July and 11 August can be shown. The predictions over Philadelphia were quite good. The simulated mixed layer temperature and humidity were usually within 1–2 K and 1–2 g kg^{-1}, respectively, of the observed for both the morning and afternoon soundings. Correlation coefficients of 0.99 and 0.98 were found for potential temperature and specific humidity, respectively, and no significant bias is evident in these figures. When the observed and simulated mixed layer depths were compared as shown in Figure 9c, somewhat more scatter was found but the correlation coefficient was still 0.96. While there was no bias in the morning mixed layer depth, there was a tendency for the model to underestimate the mixed layer

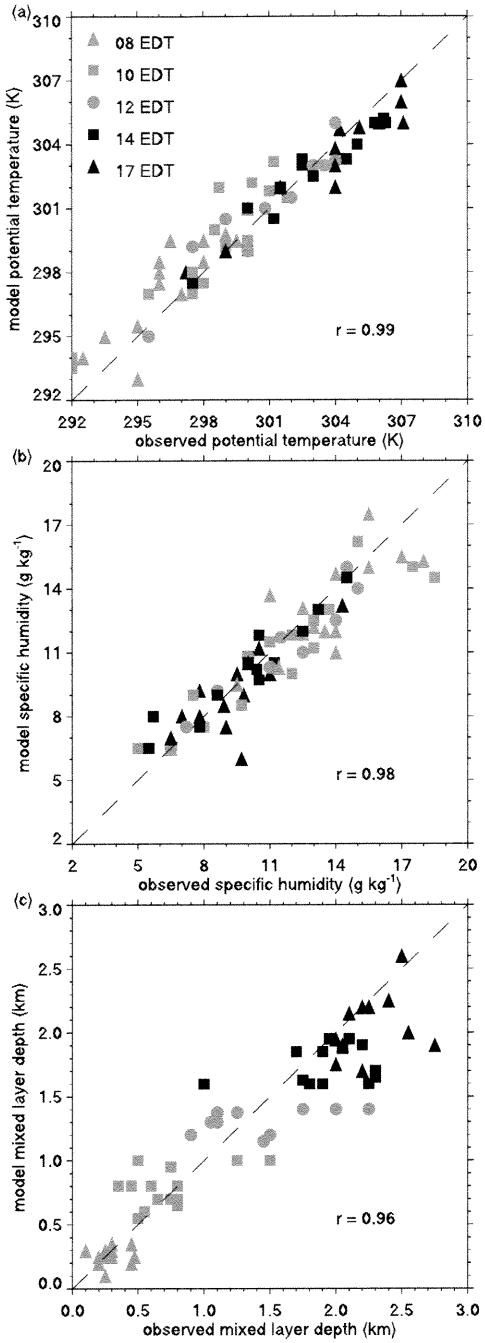

Figure 9. Scatterplot of observed and simulated average (a) potential temperature and (b) specific humidity within the mixed layer and (c) mixed layer depths. Observed values based on 65 radiosondes from site B between 23 July and 11 August.

depth during the late afternoon. This discrepancy is likely attributed to 4DDA that nudges the temperature field toward the large-scale analyses that usually do not resolve the spatial and temporal evolution of the CBL.

4.2. Air Chemistry

[32] Since the mesoscale model reproduced the main features of the observed winds and boundary layer evolution, the chemical transport model is expected to provide a reasonable estimate of regional-scale transport of pollutants over the domain shown in Figure 5 during the 30-day period. The meteorological fields in the chemical transport model were varied linearly in time with a 5-min time step, using the archived hourly output from the mesoscale model. As discussed in section 3.2, the emissions that depended on the simulated meteorological fields were updated hourly.

4.2.1. Surface observations

[33] A comparison of the resulting simulated surface ozone with observations in the vicinity of Philadelphia is shown in Figure 10. In Figure 10 the observed values from 11 stations within 50 km of the Baxter site and model results for the nine nodes closest to site B are employed. There were four periods when relatively high ozone was observed in Philadelphia, with some stations approaching or exceeding 120 ppb. These periods were 16–19 July, 23–24 July, 31 July, and 11–12 August. Except for the first day of the simulation, the model captured the diurnal and multiday evolution of ozone and the range of values in the vicinity of Philadelphia for the entire period. The afternoon ozone mixing ratios were somewhat lower than observed on some days. For the 16–19 July episode, the simulated ozone did not exceed the 130 ppb that was observed at two stations. The 24-km grid spacing employed by the model is not expected to resolve these local peaks in the spatial distribution and AIRS sites are not necessarily regionally representative. Average simulated peak afternoon values within 50 km of site B were 20 ppb or more lower than observed on 22, 27, and 28 July and 11 and 13 August. On only one day, 21 July, were the peak simulated values 20 ppb or more too high. The bias $\overline{simulated - observed}$, and gross error, $\overline{|simulated - observed|}$ over the simulation period (excluding the first two days) for the daily peak 1-hour mixing ratio were −5.8 and 12.3 ppb, respectively, while the daily peak 8-hour mixing ratio had a bias and gross error of −1.2 and 11.1 ppb, respectively.

[34] The minimum values are also well predicted, with a bias of 2.0 ppb and a gross error of 7.2 ppb over the simulation period. The minimum values usually approached zero presumably because of NO titration over the Philadelphia urban area with its relatively high emission rates. Nevertheless, relatively high minimum values were observed during the four episodes and on a few other days. Some of the high nighttime values simulated by the model (Figure 10) were the result of regional-scale ozone transport and increased turbulence associated with wind shears generated by the evolution of the low-level jet [*Corsmeier et al.*, 1997]. For example, the simulated low-level jets during the evenings of 18 and 19 July transported ozone produced from emissions in the Washington, D. C., and Baltimore area over Philadelphia.

[35] The simulated hourly ozone values were compared with up to 522 AIRS and 90 Canadian monitoring stations over the entire modeling domain. The average 1- and 8-hour maximum and 1-hour minimum ozone mixing ratios as well as the bias and gross error are shown in Figure 11. Since some "spin-up" time is required to obtain realistic results; the statistics for the first two afternoons are not plotted. When multiple ozone monitoring stations occurred within a grid cell (usually in urban areas), the average value was employed for the statistical analysis. The observed average

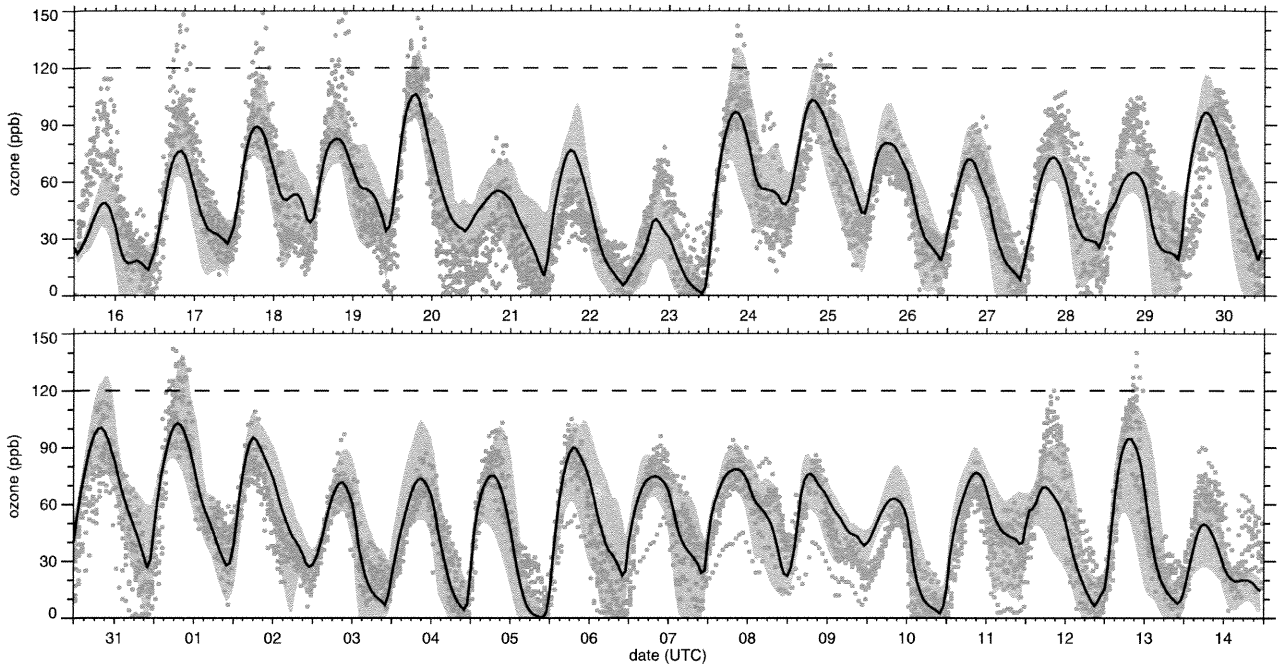

Figure 10. Time series of observed and predicted surface ozone around Philadelphia. All of the observed values (shaded dots) and the simulated range (light shading) within 50 km of site B are shown. The line is the average simulated ozone mixing ratio.

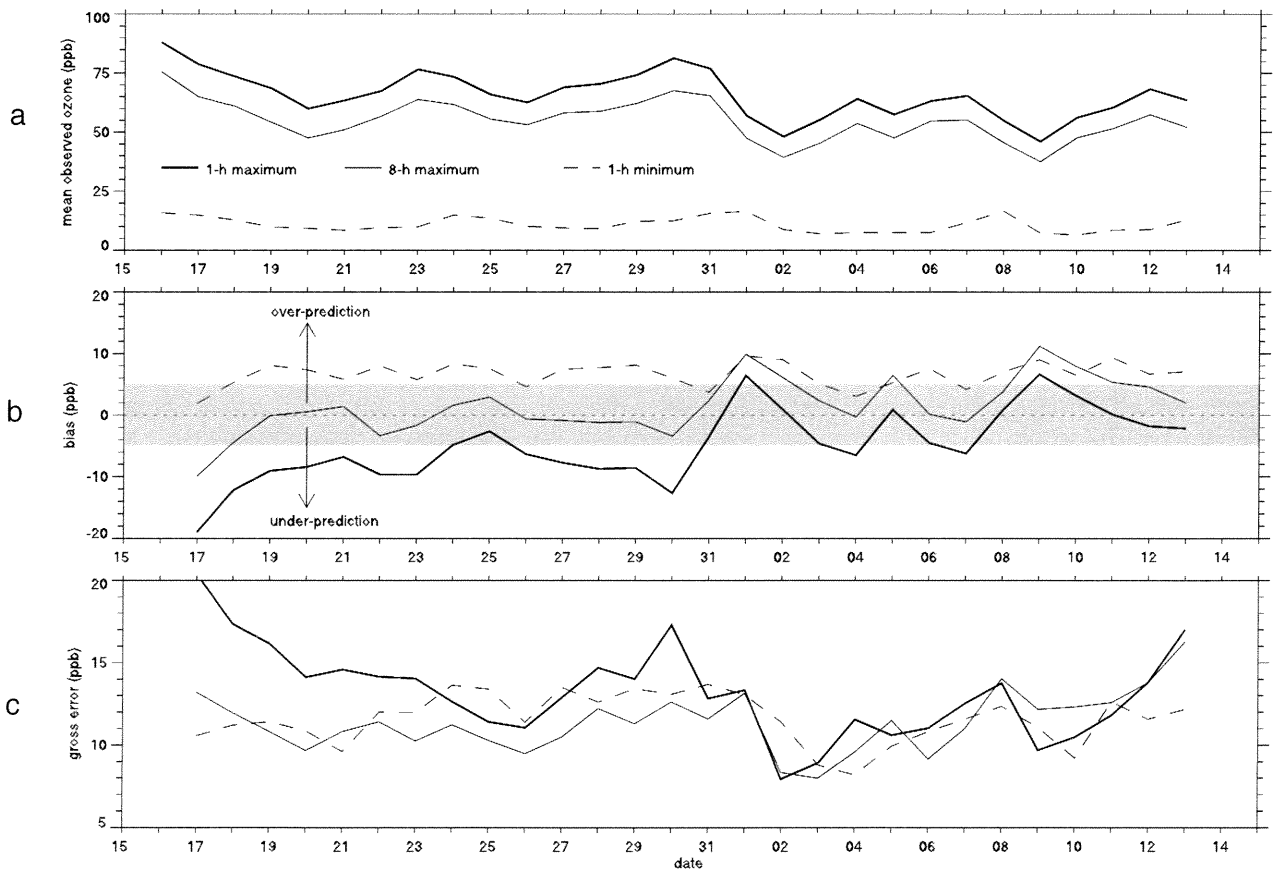

Figure 11. (a) Average observed 1- and 8-hour maximum ozone mixing ratio and 1-hour minimum ozone mixing ratio. (b) Bias and (c) gross error of the simulated quantities in Figure 11a. Shading denotes values within 5 ppb of zero.

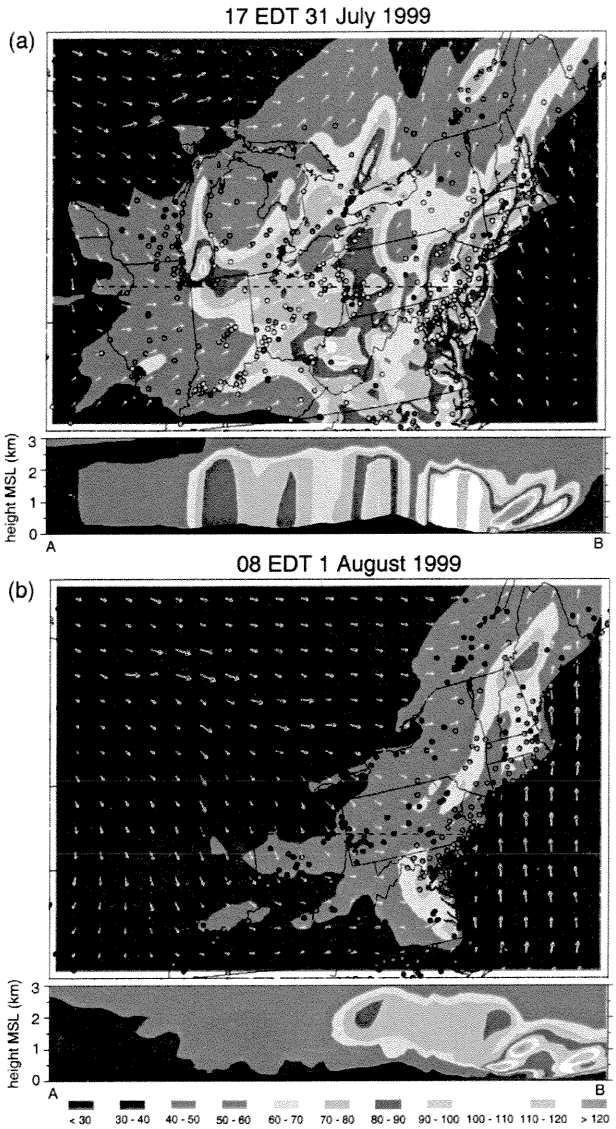

Figure 12. Observed (circles) and simulated (shaded contours) near-surface ozone and a vertical cross section of ozone through Philadelphia at (a) 1700 LT on 31 July and (b) 0800 LT on 1 August.

1- and 8-hour maximum ozone mixing ratios are shown because the magnitude of the gross error was usually proportional to the magnitude of the average ozone mixing ratios. Prior to 1 August, the 1-hour bias was between −5 and −10 ppb, indicating that the model had a tendency to underestimate the peak afternoon ozone mixing ratios. After a strong cold front moved through the area on 1 August, the average ozone mixing ratios decreased and the absolute value of the bias dropped to 5 ppb or less. The 8-hour bias was usually within ±5 ppb, with a slight tendency to overestimate the 8-hour maximum after 1 August. The daily values of the bias and gross error for the 1- and 8-hour peak ozone mixing ratios shown in Figure 11 are similar to those obtained by other chemical models [*North American Research Strategy for Tropospheric Ozone*, 2001], but the errors in the minimum values are considerably lower. The model overestimated the average minimum ozone mixing ratio over the domain by 5–8 ppb throughout the simulation period. Most of this error occurred in rural regions downwind of the major urban areas.

[36] An example of the spatial distribution of surface ozone is shown for the afternoon of 31 July and the morning of 1 August in Figure 12 to illustrate the spatial distribution of ozone and the source of the nighttime positive bias. The model produced the high ozone episode observed over the northeast urban corridor (Figure 12a). In a few regions the model overestimated (northern Indiana and southern Canada) and underestimated (Indianapolis and central Pennsylvania) the surface ozone. During the evening, the surface layer became decoupled from the air aloft (Figure 12b). Ozone was depleted near the surface while a large reservoir of ozone remained aloft by the morning of 1 August. While the simulated ozone decreased to 30 ppb or less over the western part of the domain, it remained relatively high over the northeastern United States. The surface observations from Washington, D. C., and Boston were between 40 and 60 ppb, but the horizontal extent and magnitude of the residual ozone at the surface was too large with areas greater than 50 ppb over the Appalachian Mountains. While some studies [e.g., *Aneja and Li*, 1992] have indicated that sites at higher elevations have significantly higher ozone exposure with a smaller diurnal amplitude, the AIRS monitoring stations are not necessarily representative of the conditions in complex terrain.

4.2.2. Upper-air observations

[37] Data from surface monitoring stations are usually the only observations available to evaluate air-quality models. Without information aloft, it is often difficult to determine whether the model predicts the right answer for the wrong reason or to diagnose why the model produces incorrect results. The G-1 aircraft provided measurements on 14 days of the field campaign that we employ to evaluate the evolution of air chemistry aloft that can affect surface concentrations. Since only a limited number of grid cells encompass the G-1 flight paths, especially for the local urban flights, the predictions of ozone and NO_y are compared with measurements using the approach shown in Figure 13. Shading depicts the predictions as the range of values from model grid cells when and where the aircraft typically flew. Here, 9 × 9, 5 × 5, and 3 × 3 grid cells were used for "regional," "local-to-regional," and "local" flights, respectively, around Philadelphia (Table 1). Also shown in Figure 13a are the ozonesonde profiles measured at the same time as the G-1 flights.

[38] With a few exceptions, the simulated range of ozone mixing ratios was similar to the aircraft measurements (Figure 13a). For example, on the morning of 1 August the model was 10–15 ppb higher than observed. The simulated reservoir of ozone aloft contributed to average peak values at the surface that were 10 ppb too high (Figure 10). Even though the surface values on 7 and 10 August were very close to the observations, the simulated ozone profiles aloft were somewhat higher that the aircraft data. The simulated range of ozone between 60 and 140 ppb in the vicinity of Philadelphia on 31 July, the day with the highest observed surface ozone during the aircraft operational period, agreed with the G-1 measurements. The model also produced layers of ozone aloft on the mornings of 5 and 11 August discussed previously, but the values

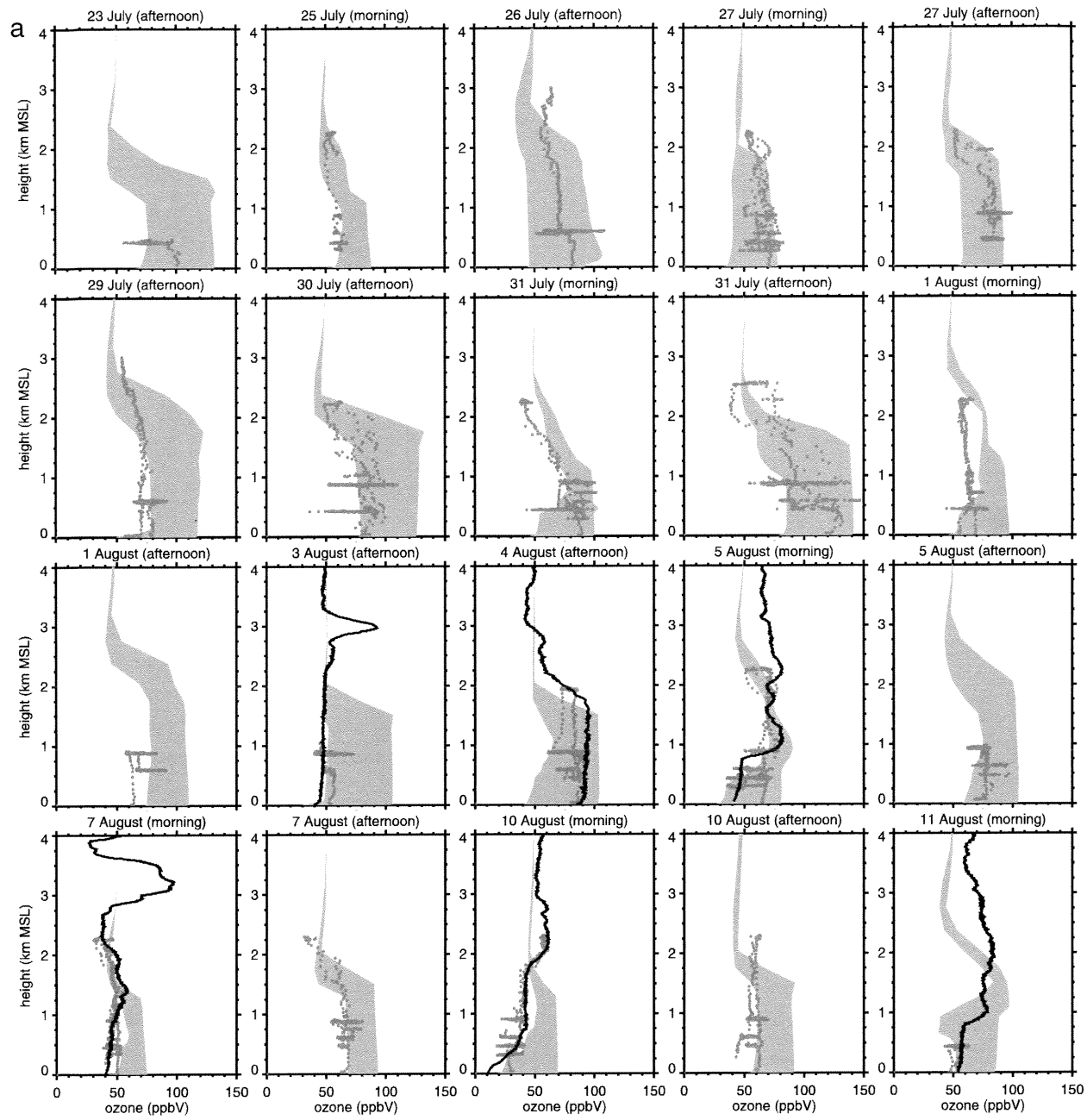

Figure 13. Observed ozone from the G-1 aircraft (shaded dots) and simulated range of ozone (light shading) in a vertical column within 24, 48, or 72 km of site B depending on whether the flight paths is "local," "local-to-regional," or "regional." respectively. The range of simulated values also encompasses the flight periods. (a) Lines are the ozonesonde profiles. (b) Same as Figure 13a except for NO_y.

above 2 km AGL are as much as 20 ppb too low. Differences between the model and the observed profiles above 2 km can be attributed to the lack of parameterized vertical mixing by convective clouds and to the constant ozone mixing ratios employed at the lateral and top boundary conditions. Long-range transport of tropospheric sources and stratosphere-troposphere exchange of ozone are processes not accounted for in this simulation that probably contribute to some of the observed variations in ozone above the CBL.

[39] While there were a number of days in which the range of observed and simulated NO_y values were similar (23, 25, and 29 July and 3, 4, and 7 August), the simulated concentration of NO_y was too low within 1 km of the surface on several days (Figure 13b). The G-1 often measured 10–50 ppb of NO_y during transects over Philadelphia within the growing CBL. Most of the simulated NO_y was composed of oxidized products, or NO_z. Concentrations of NO_x from a 4-km nested grid simulations (to be presented in another paper) were significantly higher, suggesting that urban

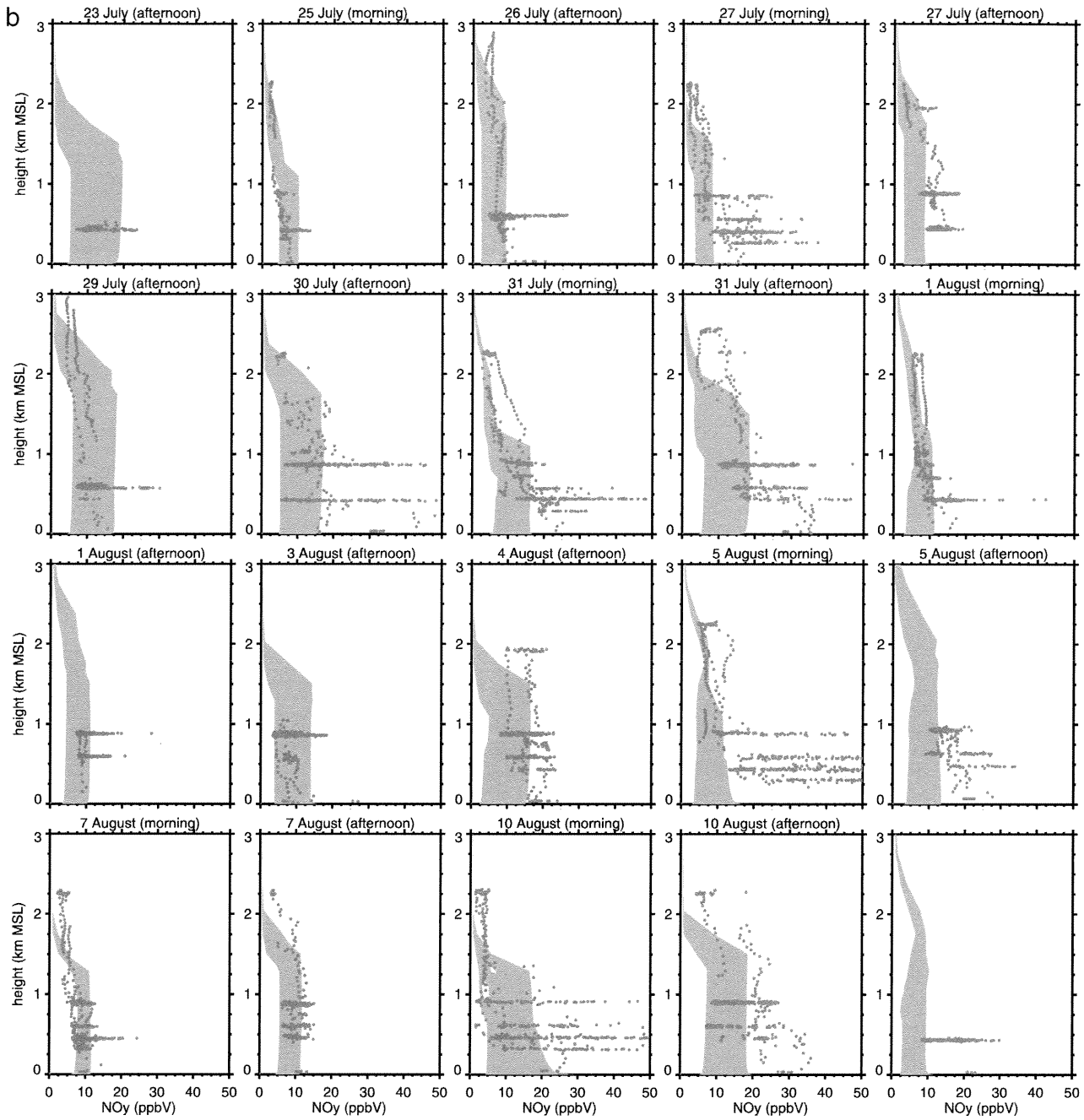

Figure 13. (continued)

emissions that are spread evenly over the 24-km grid cells smooth out the precursor concentrations of faster reacting species [*Gillani and Pleim*, 1996; *Jang et al.*, 1995].

4.3. Regional-Scale Transport

[40] In section 2 we noted in our discussion of the meteorological and ozonesonde observations that 5 and 11 August were candidate days for regional-scale transport. Having established that the model performed well, we now examine the control simulation in more detail to determine the transport processes responsible for the observed ozone layers. A series of sensitivity simulations are then presented to evaluate the impact of regional-scale transport on ozone concentrations in the vicinity of Philadelphia during the entire field campaign.

[41] The horizontal distribution of ozone predicted by the model at the time of the ozonesonde release on 5 August and on the prior afternoon is shown in Figure 14. On 4 August (Figure 14a) ozone was produced along the east coast urban corridor and mixed throughout the convective boundary layer up to 2.5 km AGL. After sunset, the ozone aloft became decoupled from the nocturnal boundary layer that developed at the surface. Ozone produced from emissions in the Washington, D. C., and Baltimore area was advected to the north into eastern Pennsylvania. During the evening as the nocturnal stable layer at the surface became

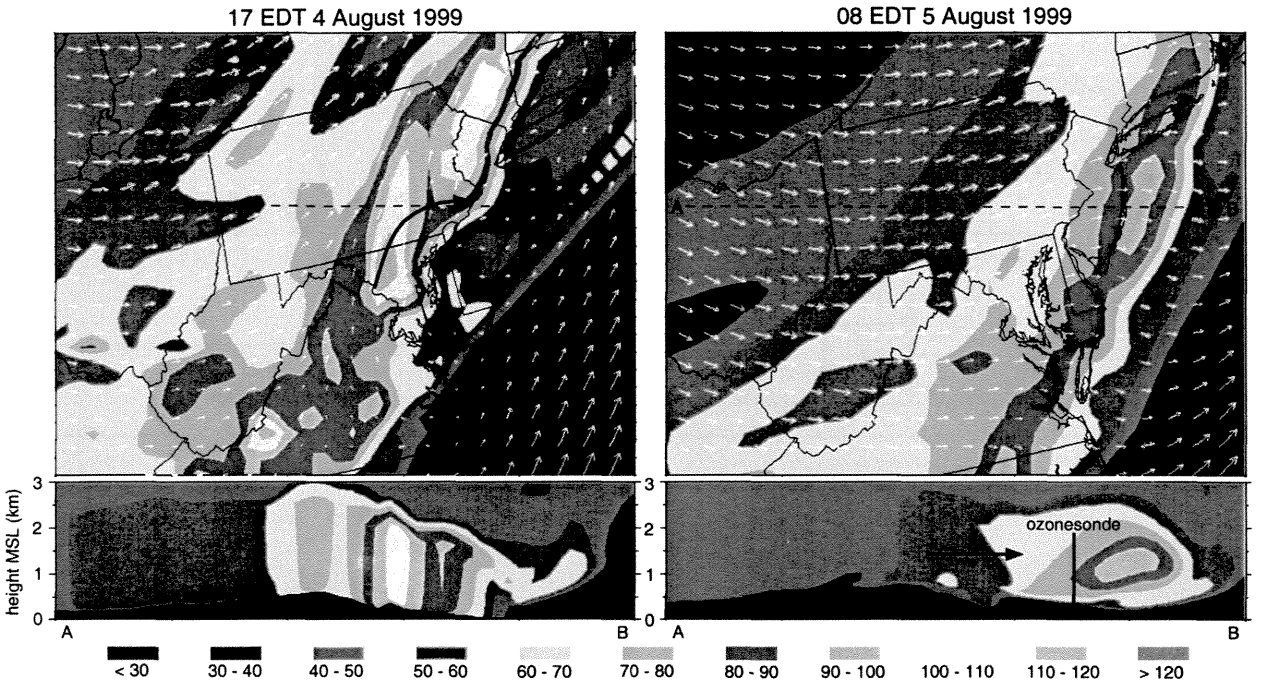

Figure 14. Simulated ozone (shaded contours) and winds (vectors) at about 1.5 km AGL and vertical cross section of ozone through Philadelphia at (a) 1700 LT on 4 August, and (b) 0800 LT on 5 August, illustrating vertical mixing and transport of ozone that produced the layer observed by the ozonesonde shown in Figures 3b and 13a. The thick arrow denotes air parcel trajectory between 1700 LT on 4 August and 0800 LT on 5 August.

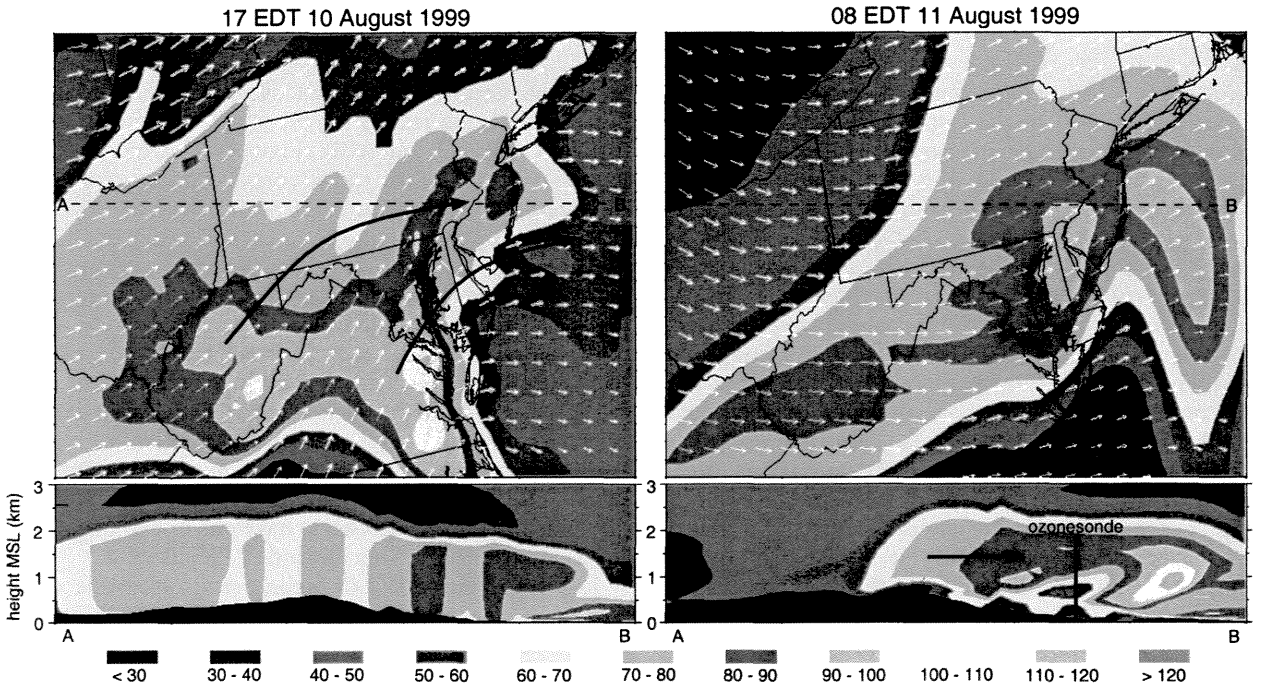

Figure 15. Simulated ozone (shaded contours) and winds (vectors) at about 1.5 km AGL and vertical cross section of ozone through Philadelphia at (a) 1700 LT on 10 August and (b) 0800 LT on 11 August, illustrating vertical mixing and transport of ozone that produced the layer observed by the ozonesonde shown in Figures 4b and 13a. The thick arrow denotes air parcel trajectory between 1700 LT on 10 August and 0800 LT on 11 August.

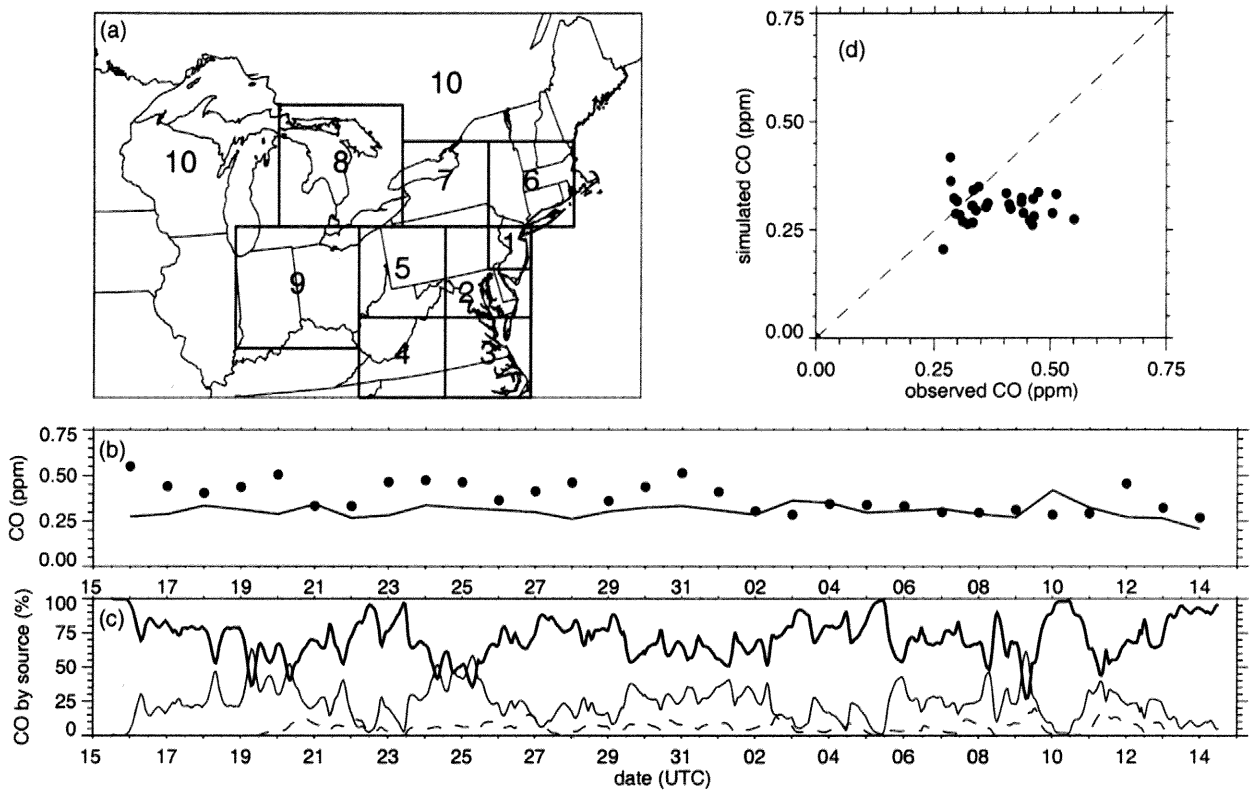

Figure 16. (a) Boxes 1–10 define how the emissions are divided during the sensitivity simulations discussed in section 4.3. Time series of (b) 24-hour average observed CO from six monitors (dots) and simulated CO (line) within 50 km of Philadelphia and (c) percent of CO from local source 1 (thick line), regional sources 2–9 (thin line), and distant source 10 (dashed line) as determined from the sensitivity simulation. (d) Scatterplot of 24-hour average observed and simulated CO shown in Figure 16b.

decoupled from the residual layer aloft, ozone at the surface was depleted by NO titration and deposition. The southwesterly winds in the late afternoon shifted to the west by the morning with the passage of a cold front in the area so that the residual layer of ozone aloft over eastern Pennsylvania (Figure 14a) was transported over Philadelphia by 0800 LT on 5 August (Figure 14b). The highest ozone mixing ratios were already transported past Philadelphia over the ocean at the time of the ozonesonde. The model results suggest that the ozonesonde was measuring within the trailing end of the ozone plume. Had the upper level winds been weaker, higher concentrations of ozone aloft would have been present over Philadelphia that could have been entrained into the growing CBL, producing higher peak values greater than the 100 ppb observed that day.

[42] A similar transport pattern occurred for the 11 August ozone layer, except that the source region of the ozone layer aloft was different and the transport distance was longer. During the late afternoon of 10 August, ozone mixing ratios between 90 and 100 ppb were produced in the CBL from the upper Ohio River valley to Chesapeake Bay (Figure 15a). Southwesterly upper level winds again shifted to the west during the evening so that ozone from the upper Ohio River valley was transported over Philadelphia. Ozone produced over Virginia and Maryland was transported over the ocean to the south and east of Philadelphia by 0800 LT on 11 August (Figure 15b). In contrast to 5 August, the ozone plume aloft is centered over the Philadelphia area. This may be the reason for the small variations in ozone between 1 and 3 km AGL (Figure 4b), while the ozone profile on 5 August had more pronounced vertical variations (Figure 3b) at the trailing edge of the ozone plume.

[43] An examination of the model results during the 30-day period suggests that different source regions contribute to ozone levels over Philadelphia on a day-to-day basis. CO is a long-lived, slowly reacting anthropogenic species that is often used as a tracer of urban air during field studies. However, we use it here to identify source regions during NE-OPS. By keeping track of the CO released from ten regions identified in Figure 16a, we can determine regional-scale source-receptor relationships during the simulation period. While the designation of the 10 source regions is arbitrary, they were selected to have one or two major urban areas in different regions upwind of Philadelphia.

[44] First, the total CO mixing ratios from the control simulation are compared with observations from six monitors located within 50 km of Philadelphia in Figures 16b and 16d. CO monitors are usually located close to urban street canyons so that the measurements are not regionally representative. In addition, the accuracy of the measurements was only 0.1 ppm for two monitors. Correlation coefficients for all pairs of CO monitors were usually below 0.1, indicating that the data is not very useful in determining regional-scale transport. To eliminate some of the problems

comparing regional-scale model output with unrepresentative CO measurements, we have instead plotted 24-hour averages among the six CO monitors and 24-hour averages of simulated CO for grid cells encompassing the monitor sites. While the overall magnitude of the simulated CO after 1 August was similar to the observed, there are still some differences that can be attributed to either unrepresentative measurements or to the simulated background value of 0.15 ppm that was too low.

[45] In Figure 16d, we show the relative contribution of the defined regions to the total CO mixing ratios. As expected, the local sources (CO source 1, Figure 16a) contributed to the largest fraction of CO over Philadelphia because of their proximity. However, there are episodes in which regional sources, as defined by the sum of CO sources 2–9, were relatively high. The high values of the regional sources between 16 and 19 July, 23 and 24 July, and 12 and 13 August correspond to three of the four high ozone episodes. The ozone episode on 31 July does not have a relatively high regional influence of CO, suggesting that local chemical production is more important on that day. The increase in regional sources (CO sources 2–9) between 4 and 5 August and between 10 and 11 August suggest that regional-scale transport contributed to the higher ozone mixing ratios observed aloft (Figures 3b and 4b). Distant sources (CO source 10) contributed between 5 and 10% of the total concentration of CO during the entire period.

[46] The specific CO source regions sampled over Philadelphia were often well correlated with the observed wind directions (Figure 6c). For example, between 15 and 19 July when strong southwesterly winds associated with the nocturnal low-level jets occurred, source regions 2 and 3 were the largest sources of CO outside of the Philadelphia area. When the winds aloft became more westerly for the periods of 23–26 July, 29 July to 1 August, and 6–9 August, source regions 5 and 9 in the Ohio River valley were relatively large. During periods of northwesterly to northerly winds over Philadelphia, such as 20 and 26 July and 2 and 9 August, source regions 7 and 8 in the Great Lakes area became relatively large. CO emissions from source region 6 that included New York City and a large portion of New England were only transported over Philadelphia on 21 July and between 2 and 5 August when the ozone concentrations were relatively low. Nevertheless, several CO source regions usually contributed to the concentrations at any one time indicating that spatially and temporally varying wind fields produced a complex mixture of pollutants along circuitous transport pathways.

[47] While the CO simulation illustrates the source regions that can contribute to pollutant episodes in Philadelphia, it cannot be used to quantify the relative contribution of local and regional sources of ozone, since the chemistry relating primary precursor pollutants and secondary pollutants, such as ozone, is complex. Therefore, three sensitivity simulations, denoted as A, B, and C, were performed with the chemical transport model using the same meteorology. Simulation A employed a local subdomain that encompasses boxes 1 and 2 in Figure 16a. Only the local emissions within the subdomain were used and the background boundary conditions from the control simulation were employed at the boundaries. In this way, regional-scale transport was eliminated, except for the transport of background concentrations of ozone. Simulation B was identical to simulation A except that the ozone produced by the control simulation was used as boundary conditions for the subdomain while the other species were held at low background values. In simulation C, the ozone precursors from the control simulation were employed as boundary conditions while ozone was held to the low background values. By comparing the control simulation results with the results from sensitivity simulations A and B, the relative contribution of ozone transport can be quantified. Simulations B and C can be compared to determine whether the air masses advected over Philadelphia are aged.

[48] The average surface ozone mixing ratios within 50 km of site B from the control simulation and the three sensitivity simulations are shown in Figure 17. The results from simulation A (local-emission simulation) was consistently lower than the control simulation and the observations, suggesting that transport was a significant factor throughout the period. An examination of the vertical ozone profiles (not shown) revealed that this simulation was missing many of the ozone layers aloft in the morning that were present in the control simulation. However, the peak concentrations on 31 July were only 20 ppb lower, suggesting that local processes were largely responsible for the high ozone concentrations on that day. Simulation B added regional ozone, but the total ozone concentrations were still not as high as the control simulation. Simulation C, which added regional ozone precursors to the local ozone production, produced 5–10 ppb more than the local-emission alone simulation, indicating that the pollutant plumes were still evolving during transit and that the air masses were not completely aged.

[49] To further quantify the effect of regional-scale transport, the relative fraction of the simulated peak daily ozone mixing ratio accounted for by each of the three sensitivity simulations is shown in Figure 18. The percentage of the ozone attributed to local sources varied between 53 and 94%. For the 16–19 July, 22–23 July, and 11–12 August ozone episodes, the fraction varied between 54 and 69%. For the 31 July episode the local contribution fraction was higher at 77%. This is consistent with the relatively low wind speeds on this day (see Figure 8a). The regional ozone transport in simulation B accounted for an increase of 28–32% for the 5 and 11 August periods described previously that had ozone layer aloft observed in the morning. While observations on these 2 days clearly indicated that regional-scale transport of ozone occurred, the model was able to quantify the relative contribution of local and regional sources and determine other days in which transport was significant.

5. Discussion

[50] Although the simulated meteorological quantities and ozone gave good quantitative agreement with the observations on most days, there were some uncertainties associated with the meteorological and chemical model. Their effects on the model results are discussed next.

[51] Although an accurate representation of cloud processes is needed in air-quality models, clouds are often the most difficult parameter to simulate by mesoscale models. Clouds directly affect the photochemical produc-

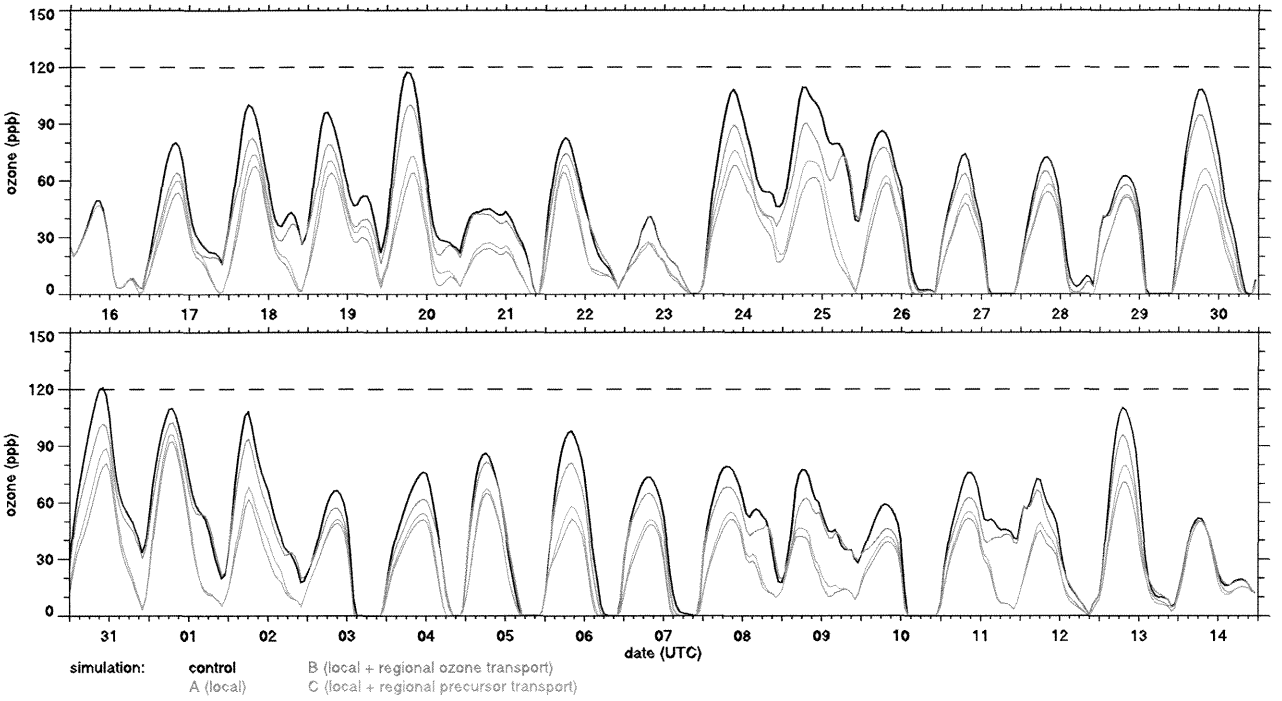

Figure 17. Simulated surface ozone from the control simulation and sensitivity simulations A (local), B (local plus regional ozone transport), and C (local plus regional precursor transport).

tion of ozone by modifying the actinic fluxes and the vertical distribution of ozone by altering mixing processes. In addition, ozone can be modified by the indirect effects of clouds through modification of boundary layer properties, such as temperature, wind speed, and mixed layer depth. While large-scale cloud mixing was included and clouds affected the photolysis rates, a subgrid-scale cloud parameterization of shallow convection [e.g., *Deng et al.*, 2000] and cloud chemistry has not been implemented yet.

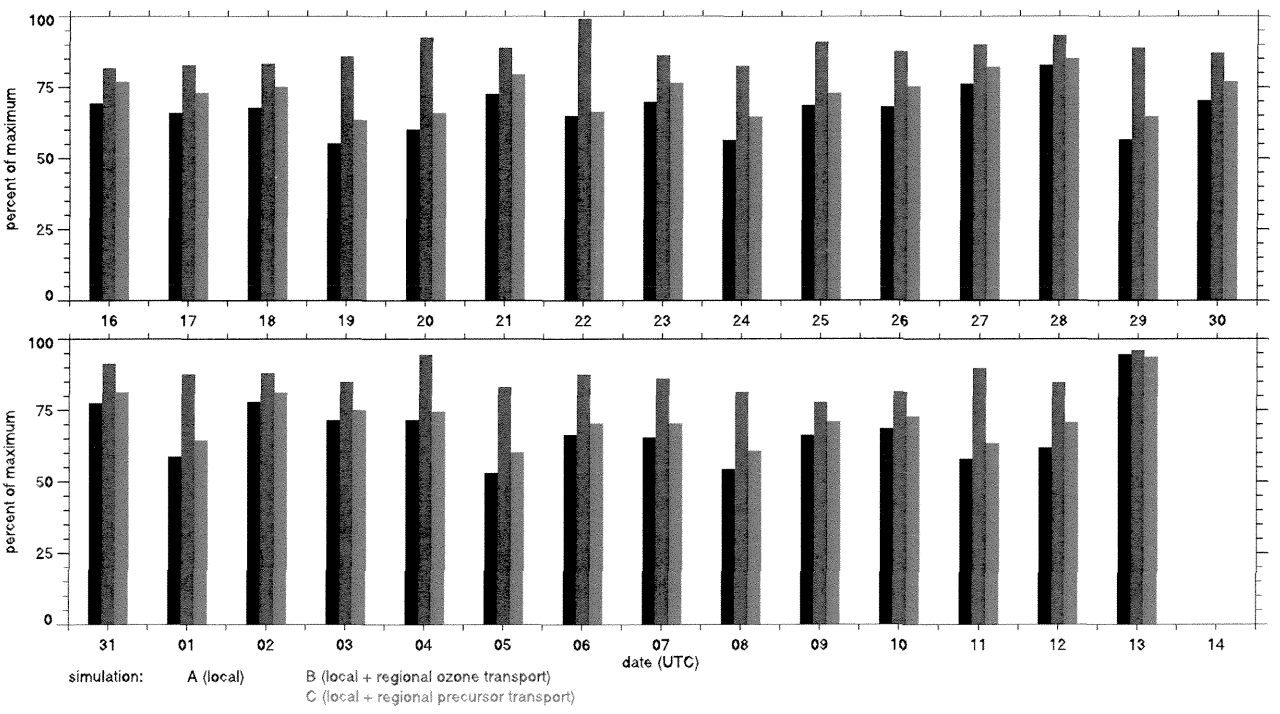

Figure 18. Ratio of the peak daytime ozone mixing ratio from sensitivity simulations A (local), B (local plus regional ozone transport), and C (local plus regional precursor transport) and the control simulation.

[52] A qualitative agreement was found between the simulated spatial distribution of cloudiness and satellite images of the observed cloud distribution throughout the 30-day period, but the amount of cloudiness can be significantly different than observed on some days for a specific location. For example, the model simulated a relatively high cloud fraction between 19 and 23 July and on 8 August associated with the passage of fronts that corresponded to the relatively low percent sunshine shown in Figure 2. However, on 24 and 28 July and 13 August the model predicted mostly clear skies over Philadelphia when the actual percent sunshine was between 15 and 50%. The differences between the observed and simulated cloud amount are not necessarily consistent with the differences between the observed and simulated ozone concentrations. On 24 July, the simulated ozone mixing ratios were similar to the observations (Figure 10) even though cloud amount was too low. On 28 July and 13 August, the simulated ozone mixing ratios were too low even though clear skies were simulated when partly to mostly cloudy skiers were observed. Despite these discrepancies, a very good agreement in ozone was found between observations and the control simulation on most days. This suggests that representing the gross features of the clouds is sufficient in simulating regional-scale ozone over a long period of time.

[53] The differences between the observed and predicted winds will have an effect on quantifying the relative contribution of local and regional sources on ozone over Philadelphia. For example, the bias of -1 m s^{-1} in the wind speeds between 0.75 and 2 km AGL suggests that the model results may overestimate the amount of ozone produced locally. Higher simulated wind speeds would advect more ozone produced locally out of the region than from the control simulation. When the winds are too low aloft, afternoon surface ozone mixing ratios can be either overestimated or underestimated depending on the location of the peak ozone concentrations aloft in the morning, as shown in Figures 14 and 15. While transport errors will affect the magnitude of the local and regional contributions shown in Figures 17 and 18, the wind errors are relatively small and are unlikely to change our conclusion that regional-scale ozone transport contributed to a significant fraction of ozone over Philadelphia. Wind speed errors will also affect the age of the simulated polluted air over Philadelphia, but the effect of ozone precursor transport is likely to still be important.

[54] The boundary conditions described in section 3.2 can also affect the model results. As shown in Figure 13a, the simulated ozone mixing ratios above 2 km are as much as 20 ppb too low on a few days. This is due primarily to the constant values employed at the lateral boundaries. In reality, the background ozone values in the middle troposphere are expected to vary over a monthlong period. One of the processes affecting tropospheric ozone is the downward transport and mixing of stratospheric ozone. For example, the ozonesonde sounding on 9 July had a layer of ozone approaching 80 ppb between 1.5 and 3 km AGL (not shown). This event occurred shortly after the passage of an upper level trough and a surface cold front. Back trajectories indicated that air parcels within this layer descended from the middle and upper troposphere over a 5-day period from northern Canada. To represent ozone variations in the middle troposphere would require coupling the model domain (Figure 5) with a continental-scale simulation that extends up to the lower stratosphere. A test simulation that increased the ozone vertical gradient at the lateral boundaries to match the average of the ozonesondes produced surface ozone mixing ratios similar to the control simulation as shown in Figure 10. The impact of downward transport from the middle troposphere on the overall surface concentrations was relatively minor compared to the production of ozone from anthropogenic and biogenic emissions. This suggests that the boundary conditions will not significantly affect the conclusions regarding the relative contribution of local and regional sources of ozone as determined by the sensitivity simulations. Still, the temporal variation of ozone in the free atmosphere may have a larger impact under different meteorological conditions.

[55] Another source of uncertainty is the spatial resolution of the model. While the 24-km horizontal grid spacing is within the range suggested by *Gillani and Pleim* [1996] to simulate regional-scale ozone, it may account for the underprediction of NO_y when compared with surface data and with G-1 observations aloft (Figure 13b). As pointed out by *Gillani and Pleim* [1996] and *Jang et al.* [1995], NO_x chemistry from point sources is complex and the concentration of NO_x and the reaction rate depends on the rate of downwind turbulent mixing. The artificial dilution of point sources or subgrid area sources by regional-scale models with horizontal grid spacings on the order of 20–80 km can lead an underestimation of NO_x. However, the model performance was better for longer-lived species, such as PAN. The simulated diurnal variation of PAN at site C ranged between 0.5 and 2 ppb in agreement with the observations (not shown). Preliminary simulations with a 4-km nested grid have shown that the predicted NO_y values were higher and much closer to the G-1 observations. For example, on 26 July the observed NO_y values were as high as 25 ppb (Figure 13b). The predicted values from the 24-km simulation were 10 ppb, while the 4-km simulation produced values as high as 22 ppb along the G-1 flight path. Predicted peak surface ozone mixing ratios were also a few ppb higher in closer agreement with the 130–150 ppb observed at two stations between 16 and 19 July (Figure 10).

[56] In this study, vertical grid resolution was a critical factor for nighttime chemistry. A simulation identical to the control simulation was performed, except that a vertical grid spacing, Δz, of 25 m at the ground was increased to 50 m. In that simulation, the nighttime surface ozone mixing ratios were significantly higher than those shown in Figure 10. We found that the vertical eddy diffusivity, K, determined by the *Mellor and Yamada* [1982] formulation was larger at night near the surface when z was twice as large as in the control simulation so that the stable boundary layer became more coupled to the air aloft. This permitted vertical mixing of ozone to replace the ozone lost through NO titration within the stable boundary layer. With a smaller z, K became smaller so that vertical mixing did not replace as much ozone lost through NO titration. While the overpredictions of the domain averaged nighttime ozone mixing ratios with a z of 25 m were between 5 and 8 ppb, they were much lower compared to the 15–25 ppb obtained from other models applied to the 1995 NARSTO-NE period [*North American Research Strategy for Tropospheric Ozone*,

2001]. The nighttime bias suggests that additional profiles of meteorological and chemical observations are needed to understand the delicate balance of ozone destruction, vertical mixing, and deposition in the nocturnal boundary layer. Developing a better understanding of mixing within the nocturnal boundary layer is the subject of considerable current research [*Doran et al.*, 2001; *Poulos et al.*, 2001].

[57] As mentioned previously, we have begun to extend this analysis to resolve small-scale processes along the east-coast urban corridor using a 4-km grid. The purpose of these simulations will be to better resolve the emissions in the urban areas and the meteorological processes affected by land/sea contrasts that will affect the ozone distribution in the immediate vicinity of Philadelphia. The results of this study will be reported in a subsequent paper.

6. Summary

[58] Measurements obtained from the NE-OPS field campaign during July and August of 1999 have been combined with results of a new meteorological and chemical model, PEGASUS, to study ozone production, transport, and mixing over northeastern United States. Good agreement between the simulations and observations was obtained, and the results have been used to illustrate transports pathways and quantify the effect of regional-scale transport of pollutants on ozone concentrations in the vicinity of Philadelphia. The principal findings from this study thus far are the following:

1. On several mornings, research aircraft and ozonesonde measurements showed concentrations of ozone significantly higher above the growing CBL than at the surface. Mixing ratios above the CBL were as much as 50 ppb higher than at the surface. The relatively strong wind speeds observed by the radar wind profilers during the evening suggest that ozone layer was transported from upwind sources over Philadelphia and not a local residual layer from the previous afternoon.

2. The results of PEGASUS compared very well with meteorological and chemical data at the surface and aloft. The average bias for ozone over Philadelphia during the 30-day period was −5.8 ppb for the peak 1-hour value during the day and 2 ppb for the minimum value at night. Over the entire domain, the average bias for the daytime peak and nighttime minimum was −4.8 and 6.6 ppb, respectively.

3. The simulation with CO tagged by source region indicates that several source regions usually contributed to the mix of pollutants over Philadelphia. Pollutants from the Ohio River valley, Great Lakes, and areas south of Philadelphia along the coast were advected into the region several times during the 30-day period.

4. A series of sensitivity simulations were performed to determine the relative contribution of ozone produced locally and ozone transported into the Philadelphia area. While the majority of the ozone was produced by emissions in the vicinity of Philadelphia and Chesapeake Bay area, as much as 30–40% of the total ozone mixing ratios could be attributed to transport from upwind locations during the high ozone episodes. The relative contribution varied from day to day.

5. Regional-scale transport contributed a significant fraction of ozone over Philadelphia for three out of the four high ozone episodes during the 30-day period. For the other episode on 31 July, local processes dominated because the wind speeds on that day were relatively low.

6. Simulated pollutant plumes were still evolving during transit from source regions to Philadelphia, indicating that the air masses were not completely aged. While ozone transport adds to local concentrations, transport of ozone precursors into the region can also contribute to local photochemical production of ozone.

[59] Since regional-scale transport and boundary layer mixing processes contributed to a large fraction of the simulated ozone over Philadelphia, these same processes likely affect the ozone concentrations in other cities along the east-coast urban corridor. The relative role of local and regional processes that affect ozone depends on location. For example, urban areas located northeast of Philadelphia are probably impacted by regional-scale transport to a greater extent because winds, that are predominantly from the southwest during the summer, would transport primary and secondary pollutants from multiple metropolitan areas. *Chamedies et al.* [1997] found that the proposed 8-hour ozone standard will require a more regional approach on U.S. pollution control strategies. The model results in this study provide evidence that regional-scale transport is another reason that emission control strategies in the northeastern U.S. need to be implemented for the entire region. Transport from upwind sources is likely to be significant under a wide range of synoptic conditions, and they can offset the reductions due to local reductions in primary emissions. When regional-scale transport of ozone was included, the model produced peak ozone mixing ratios in the vicinity of Philadelphia that exceeded the 1-hour NAAQS of 120 ppb on several days (Figure 10). The significantly lower ozone mixing ratios produced by the simulation that employed only the local emissions (Figure 17) suggests that violations of the NAAQS between 15 July and 14 August 1999 were caused by both ozone produced locally and ozone produced elsewhere.

[60] The control simulation results are currently being analyzed further to examine the transport pathways of pollutants into rural regions and the impact ozone exposure on vegetation. Additional sensitivity simulations will be performed to investigate the effects of emission control strategies and landscape changes on the production of ozone in rural areas.

Appendix A: Numerical Aspects of the Chemical Transport Model

[61] The chemical transport model solves the continuity equation for each trace gas species that includes transport, vertical diffusion, chemical production/destruction, dry deposition, and emission terms. The gas-phase chemistry in PEGASUS is modeled with the newly developed photochemical mechanism CBM-Z [*Zaveri and Peters*, 1999] that contains 53 species and 133 reactions. An operator splitting approach [*Lapidus and Pinder*, 1982] is used to solve each of the terms of the continuity equation. The RODAS3 ordinary differential equation solver of *Sandu et al.* [1997] is used for the chemical reaction calculations. A fourth-order advection form of the Bott algorithm is used for the advection terms [*Easter*, 1993]. For vertical mixing, a standard finite differ-

ence scheme with second-order spatial differencing and first-order explicit temporal differencing is used. Dry deposition is included as a lower boundary condition in the vertical mixing calculation. A series-resistance model is used to compute deposition velocities and surface resistances following *Wesely* [1989] with land use information taken from RAMS.

[62] CBM-Z is implemented using a regime-dependent approach in which the kinetics are partitioned into background, anthropogenic, and biogenic submechanisms. The background submechanism consists of the inorganic chemistry and reactions of the ubiquitous species such as the long-lived hydrocarbons methane and ethane, formaldehyde and higher aldehydes (ALD2), methanol, ethanol, and the associated radicals. The anthropogenic submechanism consists of the reactions involving organics of urban origin such as paraffins, olefins, and aromatics, while the biogenic submechanism consists of isoprene chemistry. The corresponding three atmospheric regimes are pristine, polluted, and rural. With the regime dependent approach, a submechanism is activated only if the concentration any of the species in that submechanism are nonzero or greater than a threshold value. For example, the background mechanism (pristine regime) is always active, the anthropogenic mechanism is activated in the polluted regime (usually over urban areas), and the biogenic mechanism is activated only in the rural regime (usually over forested areas where isoprene concentrations are non-zero). However, since some of the products formed in the isoprene chemistry are represented by the species in the anthropogenic mechanism, the rural regime always also activates the anthropogenic mechanism. This approach enhances the computational efficiency, and reduces the overall CPU time by up to 30% or more for large-scale simulations where all three regimes are frequently encountered.

[63] Parallelization of the chemical transport model has been developed using the Message Passing Interface (MPI) standard. The governing equations are solved using the "locally one-dimensional" approximation described by *Lapidus and Pinder* [1982], with two types of domain decomposition carried out during different steps of the integration,

Step A

$$\left.\frac{\partial C}{\partial t}\right|_{total} = \left\{ \left.\frac{\partial C}{\partial t}\right|_{x-advection} + \left.\frac{\partial C}{\partial t}\right|_{y-advection} \right\}$$

Step B

$$+\left\{ \left.\frac{\partial C}{\partial t}\right|_{z-advection} + \left.\frac{\partial C}{\partial t}\right|_{z-diffusion} + \left.\frac{\partial C}{\partial t}\right|_{chemistry} \right\}.$$

The partial notation is used to distinguish between changes to the concentration of chemical species, C, resulting from x and y transport (Step A) and vertical transport, diffusion, and local chemistry (Step B). During Step A, transport calculations along a given horizontal slab ("slab decomposition") and a set of trace gas species are assigned to each of the N available processors. This is a natural way to partition the calculations because chemical species do not interact during the time-split transport calculation, and there is no exchange of information during the horizontal transport calculations. However, transport calculations do change the horizontal gradients at each layer for each species. The processors track these change as they carry out their calculations. At the end of Step A, the resulting fields are updated among all processors, for all layers and all species. Computational description of vertical transport, vertical mixing, and chemistry (Step B) involve only local or vertical derivatives and the processor work load is based on "column decomposition." Once all the nodes have completed their calculations for chemistry and vertical transport, they pass their results to other nodes in a synchronized stacking fashion. After all the nodes have updated their chemical fields, the decomposition pattern is reconfigured and each processor then carries out the next x and y transport calculations. Tests have shown that speedup is very close to the maximum predicted by Amdahl's Law for 16 processors, with a continual improvement up to 128 processors.

[64] **Acknowledgments.** We thank the pilots and flight crew from PNNL and Stephen Springston of BNL for providing us with data from the G-1 aircraft. The ozonesonde measurements were made by Jerry Allwine and Justin Krug of PNNL. Chris Doran and Will Shaw of PNNL and Rich Coulter of ANL provided the airsonde (sites B and C) and radar wind profiler data (sites C and W). We thank Tim Starn of West Chester University for his assistance in locating site W and Barbara Turpin and Luke Oman of Rutgers University for providing the radar wind profiler data for site R. Jeff Gaffney of ANL provided the chemistry measurements at site C, John Shelton of Environment Canada provided the Canadian ozone monitoring data, and Bill Ryan of the University of Maryland provided the AIRS data. We thank Jeff Vukovich of North Carolina Supercomputer Center for generating the emissions database from SMOKE. The parallelization of the chemical transport model and generation of the day-specific emissions was supported under PNNL's Laboratory Directed Research and Development program. The Baxter radar wind profiler was operated by Pennsylvania State University with support from EPA grant R826373. This research was supported by the U.S. Department of Energy (DOE), under the auspices of the Atmospheric Sciences Program of the Office of Biological and Environmental Research, under contract DE-AC06-76RLO 1830 at the PNNL, and the U.S. Department of Agriculture Forest Service under interagency agreement NC-96-01-IA. PNNL is operated for the U.S. DOE by Battelle Memorial Institute. The Gulfstream-I aircraft is owned by Battelle Memorial Institute and operated by PNNL for the U.S. DOE.

References

Aneja, V. P., and Z. Li, Characterization of ozone at high elevation in the eastern United States: Trends, seaonal variations, and exposure, *J. Geophys. Res.*, *97*, 9873–9888, 1992.

Banta, R. M., et al., Daytime buildup and nighttime transport of urban ozone in the boundary layer during a stagnation episode, *J. Geophys. Res.*, *103*, 22,519–22,544, 1998.

Berkowitz, C. M., J. D. Fast, S. Springston, R. Larson, C. Spicer, and P. Doskey, Formation mechanisms and chemical characteristics of elevated photochemical layers over the United States, *J. Geophys. Res.*, *103*, 10,631–10,647, 1998.

Berkowitz, C. M., J. D. Fast, and R. C. Easter, Boundary-layer vertical exchange processes and the mass budget of ozone: Observations and model results, *J. Geophys. Res.*, *105*, 14,789–14,805, 2000.

Brankov, E., S. T. Rao, and P. S. Porter, A trajectory-clustering-correlation methodology for examining the long-range transport of air pollutants, *Atmos. Environ.*, *32*, 1525–1534, 1998.

Chamedies, W. L., R. D. Saylor, and E. B. Cowling, Ozone pollution in the rural U.S. and new NAAQS, *Science*, *276*, 916, 1997.

Chang, J. S., R. A. Brost, I. S. A. Isaksen, S. Madronich, P. Middleton, W. R. Stockwell, and C. J. Walcek, A three-dimensional Eulerian acid deposition model: Physical concepts and formulation, *J. Geophys. Res.*, *92*, 14,681–14,700, 1987.

Chen, C., and W. R. Cotton, A one-dimensional simulation of the stratocumulus-capped mixed layer, *Boundary Layer Meteorol.*, *25*, 289–321, 1983.

Clark, R. D., C. R. Philbrick, B. G. Doddridge, and G. A. Allen, Investigations of ozone and fine particulates in the northeast, paper presented at

Millennium Symposium on Atmospheric Chemistry, Am. Meteorol. Soc., Albuquerque, N.M., 2001.

Corsmeier, U., N. Kalthoff, O. Kolle, M. Kotzian, and F. Fiedler, Ozone concentration jump in the stable nocturnal boundary layer during a LLJ-event, *Atmos. Environ.*, *31*, 1977–1989, 1997.

Deng, A., N. Seaman, and A. Lario-Gibbs, A shallow convection scheme for 3-D regional-scale air-quality applications, paper presented at 11th Joint Conference on the Applications of Air Pollution Meteorology With the Air and Waste Management Association, Am. Meteorol. Soc., Long Beach, Calif., 2000.

Doddridge, B. G., An airborne study of chemistry and fine particulates over the U.S. mid-Atlantic region, paper presented at PM 2000: Particulate Matter and Health—The Scientific Basis for Regulatory Decision Making, Air and Waste Manage. Assoc., Charleston, S.C., 2000.

Doran, J. C., J. D. Fast, and J. Horel, The VTMX 2000 campaign, *Bull. Am. Meteorol. Soc.*, *83*, 537–558, 2001.

Duncan, B. N., and W. L. Chameides, Effects of urban emission control strategies on the export of ozone and ozone precursors from the urban atmosphere to the troposphere, *J. Geophys. Res.*, *103*, 28,159–28,179, 1998.

Easter, R. C., Two modified versions of Bott's positive definite numerical advection scheme, *Mon. Weather Rev.*, *121*, 297–304, 1993.

Fast, J. D., J. C. Doran, W. J. Shaw, R. L. Coulter, and T. J. Martin, The evolution of the boundary layer and its effect on air chemistry in the Phoenix area, *J. Geophys. Res.*, *105*, 22,833–22,848, 2000.

Finlayson-Pitts, B. J., and J. N. Pitts Jr., *Chemistry of the Upper and Lower Atmosphere*, 969 pp., Academic, San Diego, Calif., 2000.

Gery, M. W., G. Z. Whitten, J. P. Killus, and M. C. Dodge, A photochemical kinetics mechanism for urban and regional scale computer modeling, *J. Geophys. Res.*, *94*, 12,925–12,956, 1989.

Gillani, N. V., and J. E. Pleim, Sub-grid-scale features of anthropogenic emissions of NO_x and VOC in the context of regional Eulerian models, *Atmos. Environ.*, *30*, 2043–2059, 1996.

Helfand, H. M., and J. C. Labraga, Design of a nonsingular level 2.5 second-order closure model for the prediction of atmospheric turbulence, *J. Atmos. Sci.*, *45*, 113–132, 1988.

Hidy, G. M., Ozone process insights from field experiments, I, Overview, *Atmos. Environ.*, *34*, 2001–2022, 2000.

Houyoux, M. R., J. M. Vukovich, C. J. Coats Jr., N. W. Wheeler, and P. S. Kasibhatla, Emission inventory development and processing for the Seasonal Model for Regional Air Quality (SMRAQ) project, *J. Geophys. Res.*, *105*, 9079–9090, 2000.

Jang, J.-C. C., H. E. Jeffries, and S. Tonnessen, Sensitivity of ozone to model grid resolution, II, Detailed process analysis for ozone chemistry, *Atmos. Environ.*, *29*, 3101–3114, 1995.

Kleinman, L., P. H. Daum, D. G. Imre, J. H. Lee, Y.-N. Lee, L. J. Nunnermaker, S. R. Springston, J. Weinstein-Llody, and L. Newman, Ozone production in the New York City urban plume, *J. Geophys. Res.*, *105*, 14,495–14,511, 2000.

Komhyr, W. D., Electrochemical concentration cells for gas analysis, *Ann. Geophys.*, *25*, 203–210, 1969.

Komhyr, W. D., R. A. Barnes, G. B. Brothers, J. A. Lathrop, and D. P. Opperman, Electrochemical concentration cell ozonesonde performance evaluation during STOIC 1989, *J. Geophys. Res.*, *100*, 9231–9244, 1995.

Ku, J.-Y., H. Mao, K. Zhang, K. Civerolo, S. T. Rao, C. R. Philbrick, B. Doddridge, and R. Clark, Numerical investigation of the effects of boundary-layer evolution on the prediction of ozone and the efficacy of emission control options in the northeastern United States, *J. Environ. Fluid Mech.*, *1*, 209–233, 2001.

Lapidus, L., and G. F. Pinder, *Numerical Solution of Partial Differential Equations in Science and Engineering*, John Wiley, New York, 1982.

Louis, J.-F., A parametric model of vertical eddy fluxes in the atmosphere, *Boundary Layer Meteorol.*, *17*, 187–202, 1979.

Marley, N. A., J. S. Gaffney, P. J. Drayton, and R. M. Ravelo, Northeast oxidant and particulate study (NEOPS): Preliminary results from the Centerton, New Jersey field site, paper presented at Millennium Symposium on Atmospheric Chemistry, Am. Meteorol. Soc., Albuquerque, N.M., 2001.

McElroy, J. L., and T. B. Smith, Creation and fate of ozone layers aloft in southern California, *Atmos. Environ., Part A*, *27*, 1917–1929, 1993.

McKendry, I. G., D. G. Steyn, J. Lundgren, R. M. Hoff, W. Strapp, K. Anlauf, F. Froude, J. B. Martin, R. M. Banta, and L. D. Olivier, Elevated ozone layers and vertical down-mixing over the lower Fraser valley, BC, *Atmos. Environ.*, *31*, 2135–2146, 1997.

Mellor, G. L., and T. Yamada, Development of a turbulence closure model for geophysical fluid problems, *Rev. Geophys.*, *20*, 851–875, 1982.

Neu, U., T. Kunzle, and H. Wanner, On the relation between ozone storage in the residual layer and daily variation in near-surface ozone concentration: A case study, *Boundary Layer Meteorol.*, *69*, 221–247, 1994.

North American Research Strategy for Tropospheric Ozone, NARSTO model comparison and evaluation study (MCES) update, *NARSTO News*, *5*, 3–13, 2001.

Philbrick, C. R., R. D. Clark, P. Koutrakis, J. W. Munger, B. G. Doddridge, W. C. Miller, S. T. Rao, P. Geogopoulos, and L. Newman, Investigations of ozone and particulate matter air pollution in the northeast, paper presented at PM 2000: Particulate Matter and Health—The Scientific Basis for Regulatory Decision Making, Air and Waste Manage. Assoc., Charleston, S.C., 2000.

Pielke, R. A., et al., A comprehensive meteorological modeling system—RAMS, *Meteorol. Atmos. Phys.*, *49*, 69–91, 1992.

Poulos, G. S., et al., CASES-99: A comprehensive investigation of the stable nocturnal boundary layer, *Bull. Am. Meteorol. Soc.*, *83*, 555–581, 2001.

Sandu, A., J. G. Verwer, J. G. Blom, E. J. Spee, G. R. Carmichael, and F. A. Potra, Benchmarking stiff ODE solvers for atmospheric chemistry problems, II, Rosenbrock solvers, *Atmos. Environ.*, *31*, 3459–3472, 1997.

Schichtel, B. A., and R. B. Husar, Eastern North American transport climatology during high- and low-ozone days, *Atmos. Environ.*, *35*, 1029–1038, 2001.

Seaman, N. L., and S. A. Michelson, Mesoscale meteorological structure of a high-ozone episode during the 1995 NARSTO-Northeast study, *J. Appl. Meteorol.*, *39*, 384–398, 1995.

Sillman, S., The relation between ozone, NO_x, and hydrocarbons in urban and polluted environments, *Atmos. Environ.*, *33*, 1821–1845, 1999.

Solomon, P., E. Cowling, G. Hidy, and C. Furiness, Comparison of scientific findings from major ozone field studies in North America and Europe, *Atmos. Environ.*, *34*, 1885–1920, 2000.

Van Valin, C. C., J. F. Boatman, M. Luria, V. P. Aneja, D. R. Blake, M. Rodgers, and J. T. Sigmon, The compatibility between aircraft and ground-based air quality measurements, *J. Geophys. Res.*, *99*, 1043–1057, 1994.

Vukovich, F. M., Regional-scale boundary layer ozone variations in the eastern United States and their associated with meteorological variations, *Atmos. Environ.*, *29*, 2259–2273, 1995.

Wesely, M. L., Parameterization of surface resistances to gaseous dry deposition in regional-scale numerical models, *Atmos. Environ.*, *23*, 1293–1304, 1989.

Zaveri, R. A., and L. K. Peters, A new lumped structure photochemical mechanism for large-scale applications, *J. Geophys. Res.*, *104*, 30,387–30,415, 1999.

Zhang, J., and S. T. Rao, On the role of vertical mixing in the temporal evolution of the ground-level ozone concentrations, *J. Appl. Meteorol.*, *38*, 1674–1691, 1999.

Zhang, K., H. Mao, K. Civerolo, S. Berman, J.-Y. Ku, S. T. Rao, B. Doddridge, C. R. Philbrick, and R. Clark, Numerical investigations of boundary layer evolution and nocturnal low-level jets: Local versus nonlocal PBL schemes, *J. Environ. Fluid Mech.*, *1*, 171–208, 2001.

X. Bian, E. G. Chapman, R. C. Easter, J. D. Fast, and R. A. Zaveri, Pacific Northwest National Laboratory, 902 Battelle Boulevard, P. O. Box 999, Richland, WA 99352, USA. (xbian@fs.fed.us; elaine.chapman@pnl.gov; richard.easter@pnl.gov; jerome.fast@pnl.gov; rahul.zaveri@pnl.gov)